ELSEVIER

Contents lists available at ScienceDirect

# **Environment International**

journal homepage: www.elsevier.com/locate/envint





# Variation in chemical composition and sources of PM<sub>2.5</sub> during the COVID-19 lockdown in Delhi

Chirag Manchanda <sup>a</sup>, Mayank Kumar <sup>a,\*</sup>, Vikram Singh <sup>b,\*</sup>, Mohd Faisal <sup>b</sup>, Naba Hazarika <sup>c</sup>, Ashutosh Shukla <sup>d</sup>, Vipul Lalchandani <sup>d</sup>, Vikas Goel <sup>a</sup>, Navaneeth Thamban <sup>d</sup>, Dilip Ganguly <sup>e</sup>, Sachchida Nand Tripathi <sup>d,\*</sup>

- <sup>a</sup> Department of Mechanical Engineering, Indian Institute of Technology Delhi, New Delhi, India
- <sup>b</sup> Department of Chemical Engineering, Indian Institute of Technology Delhi, New Delhi, India
- <sup>c</sup> Department of Applied Mechanics, Indian Institute of Technology Delhi, New Delhi, India
- d Department of Civil Engineering, Indian Institute of Technology Kanpur, Uttar Pradesh, India
- e Centre for Atmospheric Sciences, Indian Institute of Technology Delhi, New Delhi, India

# ARTICLE INFO

Handling Editor: Xavier Querol

Keywords:
COVID-19 lockdown
Source apportionment
PM2.5
Delhi
Air pollution
Elemental and organic fractions

#### ABSTRACT

The Government of India (GOI) announced a nationwide lockdown starting 25th March 2020 to contain the spread of COVID-19, leading to an unprecedented decline in anthropogenic activities and, in turn, improvements in ambient air quality. This is the first study to focus on highly time-resolved chemical speciation and source apportionment of PM2.5 to assess the impact of the lockdown and subsequent relaxations on the sources of ambient PM<sub>2.5</sub> in Delhi, India. The elemental, organic, and black carbon fractions of PM<sub>2.5</sub> were measured at the IIT Delhi campus from February 2020 to May 2020. We report source apportionment results using positive matrix factorization (PMF) of organic and elemental fractions of  $PM_{2.5}$  during the different phases of the lockdown. The resolved sources such as vehicular emissions, domestic coal combustion, and semi-volatile oxygenated organic aerosol (SVOOA) were found to decrease by 96%, 95%, and 86%, respectively, during lockdown phase-1 as compared to pre-lockdown. An unforeseen rise in O3 concentrations with declining NOx levels was observed, similar to other parts of the globe, leading to the low-volatility oxygenated organic aerosols (LVOOA) increasing to almost double the pre-lockdown concentrations during the last phase of the lockdown. The effect of the lockdown was found to be less pronounced on other resolved sources like secondary chloride, power plants, dustrelated, hydrocarbon-like organic aerosols (HOA), and biomass burning related emissions, which were also swayed by the changing meteorological conditions during the four lockdown phases. The results presented in this study provide a basis for future emission control strategies, quantifying the extent to which constraining certain anthropogenic activities can ameliorate the ambient air. These results have direct relevance to not only Delhi but the entire Indo-Gangetic plain (IGP), citing similar geographical and meteorological conditions common to the region along with overlapping regional emission sources.

Summary of main findings: We identify sources like vehicular emissions, domestic coal combustion, and semi-volatile oxygenated organic aerosol (SVOOA) to be severely impacted by the lockdown, whereas ozone levels and, in turn, low-volatility oxygenated organic aerosols (LVOOA) rise by more than 95% compared to the pre-lockdown concentrations during the last phase of the lockdown. However, other sources resolved in this study, like secondary chloride, power plants, dust-related, hydrocarbon-like organic aerosols (HOA), and biomass burning related emissions, were mainly driven by the changes in the meteorological conditions rather than the lockdown.

# 1. Introduction

The progression of air pollutants from their source to the receptor is

governed by a multitude of transport processes (advective winds, convective updraft, or turbulent diffusion) and multiphase transformations. These transformations are often effected by chemical

E-mail addresses: kmayank@mech.iitd.ac.in (M. Kumar), vs225@chemical.iitd.ac.in (V. Singh), snt@iitk.ac.in (S.N. Tripathi).

https://doi.org/10.1016/j.envint.2021.106541

<sup>\*</sup> Corresponding authors.

reactions that lead to heterogeneous mass transfer, which further complicates the system. Thus the concentration of each pollutant is often dependent on the concentration of other pollutants through a series of chemical reactions (Seinfeld, 2004). Time-resolved measurements of the concentration and chemical composition of these aerosols provide valuable insights into the levels of air pollution (Fehsenfeld, 2004). However, measurements alone are limited in space and time and are unable to provide much information on the origin or source of these pollutants. This has led to the widespread use of various data analysis/ source apportionment techniques in the last few decades to extract more information on the nature and composition of emission sources (Watson and Chow, 2015). However, secondary pollutants display a highly nonlinear relationship with precursor emissions; thus, source apportionment techniques are unable to provide any definitive information to predict the effect of increase/decrease of precursor emissions on secondary pollutant concentrations (Burr and Zhang, 2011).

The COVID-19 induced lockdown around different parts of the globe resulted in an unprecedented impact on the environment, with a drastic reduction in primary emissions; thus, enabling us to evaluate the impact of reduced precursor concentrations on primary and secondary aerosols, allowing us to better understand the dominant formation mechanism for a particular secondary pollutant in a given setting. The first lockdown was enforced in various parts of the Hubei province in China from 23rd January 2020, followed by similar measures in other cities (Wu et al., 2020). The COVID-19 outbreak was declared to be a pandemic by the World Health Organization (WHO) on 11th March 2020 (Sohrabi et al., 2020), following which lockdown or similar restricted movement measures were implemented in almost every region across the globe, although with varying stringency (Oxford COVID-19 Government Response Tracker, 2020).

An early study by Bao and Zhang (2020) analyzed the impact of reduced human mobility due to the lockdown on ambient air quality in 44 cities in Northern China from January to March 2020. The study found the average AQI to decrease by 7.8%, while significant pollutants like SO<sub>2</sub>, PM<sub>2.5</sub>, PM<sub>10</sub>, NO<sub>2</sub>, and CO, decreased 6.76%, 5.93%, 13.66%, 24.67%, and 4.58%, respectively. A consequent study by Li et al. (2020) utilized the Particulate Source Apportionment Technology (PSAT) coupled with the Comprehensive Air Quality Model with extensions (CAMx) to quantify contributions from 8 different sources to total PM<sub>2.5</sub> variations over the Yangtze River Delta (YRD) region, with the study period spanning 1st January to 31st March 2020 and the most stringent lockdown lasting from 24th January to 25th February 2020. Significant reductions in industrial operations, vehicular kilometers traveled (VKT), construction, and other anthropogenic activities were observed, in turn, bringing about a 25.4% to 48.1% decrease in PM<sub>2.5</sub> concentrations at different sites over the YRD region. However, an average rebound of 20.5% was recorded for ozone concentration. This anomaly was attributed to the fact that a significant drop in the NO<sub>x</sub> concentration was observed (29.5% to 51.7%). At the same time, the reduction in VOC was not as intense as NO<sub>x</sub> leading to a drop in titration effect towards ozone (Seinfeld and Pandis, 2006).

Such increase in regional oxidation capacity effected by the rise in ozone concentration due to decrease in  $NO_x$  in a VOC-limited environment during the lockdown was also reported by several other independent studies, such as Lv et al. (2020) for Beijing (China); Zheng et al. (2020) for Wuhan (China); Sicard et al. (2020) for Wuhan (China), Nice (France), Rome (Italy), Turin (Italy), Valencia (Spain); Tobías et al. (2020) for Barcelona (Spain); Mahato et al. (2020) for Delhi (India), Selvam et al. (2020) for Gujrat (India), Kumari and Toshniwal (2020) for Delhi (India) and Mumbai (India).

In India, the nationwide lockdown was implemented on 24th March 2020 and lasted up till 31st May 2020, with phase-wise relaxations starting 19th April 2020. Mahato et al. (2020) published an early work quantifying the impact of the first phase of the lockdown on ambient air quality in the Delhi-NCT region. The study reported average  $PM_{2.5}$  and  $PM_{10}$  concentrations to dip by 53% and 52% respectively when

compared to the pre-lockdown, while  $SO_2$ ,  $NO_2$ , CO, and  $NH_3$  were found to decrease by 18%, 53%, 30%, and 12%, respectively. Similar trends in  $PM_{2.5}$ ,  $SO_2$ ,  $NO_2$ , and CO concentrations were observed independently by Srivastava et al. (2020) in both Lucknow and Delhi, by Kumari and Toshniwal (2020) in Delhi, Mumbai, and Singrauli, and by Selvam et al. (2020) in Gujrat. However, the reduction in  $SO_2$  was found to be more pronounced in Mumbai (39%) Gujarat (48%) and was attributed to their closeness to the ocean and, thus, shipping emissions by Selvam et al. (2020) and Kumari and Toshniwal (2020).

Despite these early studies investigating the impact of the lockdown in India, there has been no study focusing on the variation of the sources and chemical composition of particulate matter during different phases of the lockdown or the impact of increased  $\rm O_3$  concentrations on the sources of PM<sub>2.5</sub>. The present study is aimed at studying the highly timeresolved variation of sources contributing to both the organic and inorganic fragments of PM<sub>2.5</sub> along with black carbon, from prelockdown through each phase of the lockdown. These results aid us in quantifying the impact that reduction of certain primary emissions can have on overall air quality and the inadvertent effect these reductions can have on secondary aerosols. This study also extends the double positive matrix factorization (PMF) methodology proposed by Petit et al., (2014) to account for elemental, organic, and black carbon fractions of PM<sub>2.5</sub> in a single source apportionment analysis and utilize the elemental tracers to aid in understanding the source of organic aerosols.

# 2. Experimental methods and data analysis

#### 2.1. Sampling site and instrumentation

The sampling was conducted at the campus of Indian Institute of Technology (IIT), Delhi ( $28^{\circ}32'N$ ;  $77^{\circ}11'E$ ). The instruments are housed in a temperature-controlled laboratory on the top floor of a four-story building on campus. The nearest source of local emissions is an arterial road outside campus, located about 150 m from the building.

The nationwide lockdown was implemented in India for an initial period of 21 days, starting 25th March 2020 until 14th April 2020. The lockdown was extended for another 21 days until 3rd May 2020, with the first set of relaxations to certain agricultural and industrial activities, beginning 20th April 2020. Following the end of lockdown phase-2, the lockdown was further extended twice for a period of 14 days each, with increased allowances focused on restarting commercial activities before concluding on 31st May 2020. Further details about the allowances in each phase of the lockdown have been discussed in supplementary information (SI) section 3.

The study period has been subdivided into five phases, such that each subsequent phase coincides with increasing relaxations in the lockdown: Pre-Lockdown (PLD) (24th February – 24th March 2020), effective Lockdown Phase-1 (eLD-1) (25th March -19th April 2020), effective Lockdown Phase-2 (eLD-2) (20th April – 3rd May 2020), Lockdown Phase-3 (LD-3) (4th May – 17th May 2020), Lockdown Phase-4 (LD-4) (18th May – 31st May 2020).

The Xact 625i, XRF-based ambient metals monitor (Cooper Environmental Services, Tigard, Oregon, USA) equipped with a PM $_{2.5}$  inlet was deployed for sampling and was set up to quantify 36 elements with an hourly time resolution. Meanwhile, an Aerosol Chemical Speciation Monitor (ACSM, Aerodyne Inc., MA, USA) was deployed for analyzing the non-refractory particulate matter with an aerodynamic diameter smaller than 2.5  $\mu m$  (NR-PM $_{2.5}$ ). The ACSM measured the concentration of organic aerosols along with sulfate, nitrate, ammonium (SNA), and chloride concentration, with a time resolution of ten minutes, averaged to an hourly time scale. Black Carbon (BC) concentrations were measured using a multichannel Aethalometer (Magee Scientific Model AE33, Berkeley, CA) with a 2.5  $\mu m$  inlet cut and a 1-minute time resolution.

Total  $PM_{2.5}$  was measured using a collocated Beta Attenuation Monitor (BAM 1022, MetOne Instruments Inc., OR, USA), with a 15-min

time resolution, due to technical difficulties faced during the lockdown, the data was only available for the PLD and LD-3 phase and is used for data quality assurance or quality control (QA/QC) purposes (Figure S1), Wind Speed (WS) and Wind Direction (WD) were calculated for the nearest grid point to the sampling site, using the Global Forecast System (GFS, NCEP, USA). Relative Humidity (RH), Ambient Temperature (AT), and rainfall were recorded using an onsite Ambient Weather Monitoring station. Ozone, SO<sub>2</sub>, CO, and NO<sub>x</sub> measurements were taken from the Continuous Ambient Air Quality Monitoring Station (CAAQMS) at RK Puram, located at a distance of around 3 km from our sampling site. All CAAQMS stations in Delhi, including the RK Puram station, are managed by either the Central Pollution Control Board (CPCB) or the Delhi Pollution Control Council (DPCC) and together provide a network of near-real-time monitoring of PM2.5 and PM10 levels, along with major gaseous pollutants. Further details on the instrumentation and QA/QC checks for each instrument are provided in SI section S1.

# 2.2. Source apportionment using PMF

This study utilizes Positive Matrix Factorization (PMF) (Paatero and Tapper, 1994) to apportion the measured particulate concentrations to realizable sources. PMF is a standard multivariate factor analysis tool widely used for source apportionment of aerosols (Sharma et al., 2016; Ulbrich et al., 2009; Vossler et al., 2016). The algorithm attempts to best describe the variability in a multivariate input dataset as the linear combination of a set of constant factor profiles and their relative contribution at every corresponding time step, as shown in Eq. (1):

$$x_{ij} = \sum_{k=1}^{p} g_{ik} f_{kj} + e_{ij} \tag{1}$$

Where  $x_{ij}$  is the measured elemental concentration,  $f_{kj}$  is the factor/source profile,  $g_{ik}$  the time-varying contribution of each source, and  $e_{ij}$  represent the elements of the residuals matrix. The indices i and j denote each of the n time steps and m chemical species, while k refers to each factor/source out of total p source profiles, which is defined by the user.

In PMF, each element of the factor matrix is constrained that no sample can have a negative factor contribution. The solution to Eqn. (1) is achieved iteratively by minimizing the object function or the goodness of fit parameter known as Q value:

$$Q = \sum_{i} \sum_{j} \left(\frac{e_{ij}}{s_{ij}}\right)^{2} \tag{2}$$

Here,  $s_{ij}$  corresponds to the measurement uncertainty for every cell of the input matrix  $x_{ij}$ . The PMF algorithm was solved using the Multilinear Engine (ME)-2 (Paatero, 1999). In this study, the PMF algorithm was implemented using EPA PMF 5.0 that is built on the ME-2 solution model. A detailed description of the model is provided in past studies (Paatero, 1997; Paatero and Tapper, 1994).

As discussed in section 1, the present study extends on the double PMF method, initially proposed by Petit et al. (2014). Petit and coworkers proposed to deconvolve the organic aerosol (OA) mass spectra using the routine PMF as described above, followed by a second PMF taking the deconvolved OA factors in conjunction with black carbon and inorganic ions like sulfate, nitrate, and ammonium as input. In the present study, we follow the same steps as proposed by Petit et al., (2014); however, instead of the inorganic ions, we use the elemental measurements made by the Xact 625i in conjunction with black carbon measurements and deconvolved OA mass spectra, for input to the PMF at the second step. Further details on PMF input preparation, factor selection, and uncertainty quantification for both the routine PMF and the double PMF have been reported in SI section S2.

#### 3. Results and discussion

The PLD phase in the present study marks the phase with no restricted movement, while eLD-1 corresponds to the phase with the most stringent lockdown. Consequently, the span of each phase from eLD-2 to LD-4 has been concomitant with increments in relaxations to the lockdown (resulting in increased commercial activity and human mobility) as implemented by the state/central government.

Variation in instrument total PM<sub>2.5</sub> and its constituents, along with the major gaseous pollutants for both during the lockdown in 2020 and the same period in 2019, is presented in Fig. 1 (a-d). The instrument total PM<sub>2.5</sub> represents the sum total of the elemental, organic, and black carbon fractions of PM2.5 measured using Xact 625i, q-ACSM, and Aethalometer AE33, respectively. The instrument total PM2.5 includes the metals and chlorine measurements from the Xact, the organics and the inorganic ions (sulfate, nitrate, ammonium) from ACSM and BC from Aethalometer. The instrument total PM<sub>2.5</sub> has been compared with total PM<sub>2.5</sub> measured by a co-located BAM, and both have been found to have appreciable correlation (Pearson R > 0.91) and low residual mass (less than 10%) (Figure S1). Considering the temporal variation of PM<sub>2.5</sub> during the lockdown phases (Fig. 1(a)), we note that the average PM<sub>2.5</sub> values fall by 53.6% from PLD to eLD-1; this is in line with the findings of recent studies investigating the impact of the lockdown on PM<sub>2.5</sub> levels in Delhi (Dhaka et al., 2020; Kumar et al., 2020; Mahato et al., 2020; Yadav et al., 2020). The PM levels trend back towards the initial concentrations with increasing relaxations in subsequent phases of the lockdown; however, even during LD-4, average PM2.5 remained 33% lower compared to the PLD values. Considering the PM<sub>2.5</sub> levels in 2019 (Fig. 1(a)), we see that the average total PM<sub>2.5</sub> during the time period corresponding to eLD-2 to LD-4 (April to May 2019) is lower than what is observed during February to March 2019, even without the lockdown. This variation observed in 2019 potentially stems from meteorological parameters like boundary layer height, temperature, and RH, varying across seasons or due to the seasonal nature of some emission sources. Comparing the PM levels in 2020 with the corresponding periods in 2019; the average PM<sub>2.5</sub> levels were lower in 2020 by 27.8%, 53.1%, 36.8%, 34%, and 18% for each of PLD, eLD-1, eLD-2, LD-3, and LD-4. These observations highlight the fact that any reduction during a lockdown phase in comparison with PLD cannot be attributed to as an impact of the lockdown alone, as that would undermine the inherent seasonal impact on the PM levels as observed for 2019. However, taking previous years' levels as reference for reduction during the lockdown cannot be justified either, as it can be seen that the PM levels in 2020 during PLD were ~28% lower compared to 2019; so while comparing with previous year levels may account for seasonal variation, it will discard any increase or decrease in source emission across the two years.

Taking note of the temporal variation of the gaseous pollutants, a significant drop in NO2, NO, and CO concentrations 56%, 90%, and 32% (Figure S6(a)) respectively, was recorded during eLD-1 w.r.t PLD, while SO<sub>2</sub> remains largely unaffected by the lockdown. Comparing the levels of gaseous pollutants during the lockdown with the levels in 2019 (Fig. 1 (c) and Fig. 1(d)),  $SO_2$  in 2020 during the study period remains  $\sim 78\%$ higher than the 2019 levels, reaching the highest in LD-4, where the average levels are around 2.8 times compared to the same period in 2019. NO2 and CO are on average 60.5% and 67% lower than their average levels in 2019, with the lowest during eLD-1with ~73% reduction as compared to 2019, highlighting the impact of the lockdown. NO concentration levels during the study period when compared to 2019, are severely impacted by the lockdown, while the average concentrations in 2020 are 46% less than 2019 during PLD, the average levels are 93% lower in 2020 w.r.t 2019 during elD-1 to LD-4. Further discussion on time variations of these gaseous pollutants is presented in SI section 3.1.2.

The effect of the lockdown on secondary aerosol formation is further analyzed using the Sulfate Oxidation Ratio(SOR) and Nitrate Oxidation Ratio (NOR) (Fig. 1(d)). The SOR and NOR are defined as the molar ratio

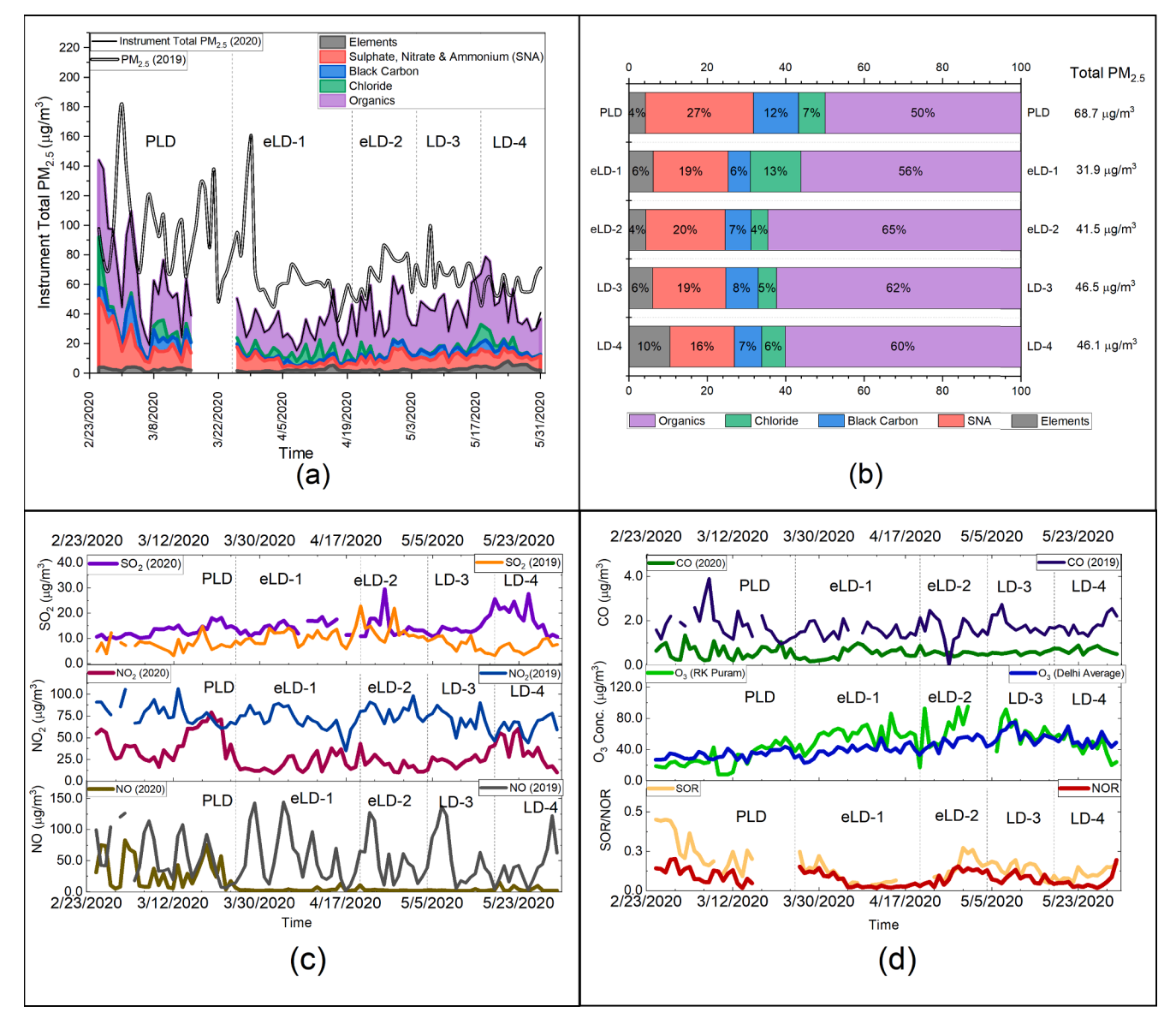


Fig. 1. Effect of the lockdown on gaseous pollutants and particulate matter, (a) Time variation of instrument total  $PM_{2.5}$  and its major constituents and its comparison with  $PM_{2.5}$  levels during corresponding period in 2019 (Instrument Total  $PM_{2.5}$  elemental  $PM_{2.5}$  (Xact) + SNA (ACSM) + Chloride (Xact) + Black Carbon (Aethalometer)); (b) Phase-wise composition of measured  $PM_{2.5}$ ; (c) Time variation of  $SO_2$ ,  $SO_2$ , NO (top to bottom) in 2020 and 2019 for corresponding period; (d) Time variation of  $SO_2$ ,  $SO_3$  (at RK Puram and average for Delhi), SOR and SOR (top to bottom) in 2020 and 2019 for corresponding period.

of  $SO_4$  and  $NO_3$  to total oxidized S ( $SO_4 + SO_2$ ) and total oxidized N ( $NO_3 + NO_x$ ), respectively (Zhang et al., 2011). The average SOR for the PLD was 0.26, followed by 0.1, 0.15, 0.13, and 0.1 for each of eLD-1 to LD-4, while the average NOR for the PLD was 0.12, followed by 0.07, 0.1, 0.1, and 0.06 for each of eLD-1 to LD-4. According to previous studies, SOR and NOR lower than 0.25 and 0.10, respectively, are a marker for primary particulate matter (Ohta and Okita, 1990). Thus, the reduction in these ratios seems to indicate some role of lockdown in hindering the formation of secondary particles. However, contrary to the nature of total  $PM_{2.5}$  and gaseous pollutants, these ratios do not tend towards the PLD values; with increasing relaxations, these ratios achieve the lowest average values in LD-4.

In Fig. 1 (d), we also note that the behavior of  $O_3$  doesn't reconcile with the trend followed by total  $PM_{2.5}$  and other gaseous pollutants discussed above and are found to increase by 98%, 121%, 118%, and 54% in each of eLD-1 to LD-4 w.r.t the PLD concentrations (Figure S6 (a)). Similar, anomalies in terms of increase in ozone concentration following the lockdown have been observed in some recent studies, not

only in India but also in different parts of China, France, Italy, and Spain (Sicard et al., 2020; Tobías et al., 2020; Zheng et al., 2020) and have attributed the increase in ozone to the reduction of NO<sub>x</sub> in a VOC-limited environment (Monks et al., 2015). This non-linear coupling between VOC, NOx, and O3 was originally discussed in an early study by Finlayson-Pitts and Pitts (1993). However, it is also interesting to note that despite the increasing NO<sub>x</sub> concentrations in LD-4 and high O<sub>3</sub> concentrations during the same period, NOR remains 0.06, indicating low concentrations of particulate nitrate. The same scenario has been discussed by Finlayson-Pitts and Pitts (1993), presenting the hypothesis that VOC and NO<sub>x</sub> compete for OH radicals for oxidation. When the VOC to NO<sub>x</sub> ratio increases (decreasing NO<sub>x</sub> at constant VOC), the oxidation of VOC is favored over NOx, resulting in lower nitrate concentrations. Similarly, for SO<sub>2</sub> and associated lower sulfate indicated by low SOR despite high O3, gas-phase oxidation of SO2, similar to NO2, competes for the OH radical, while aqueous phase oxidation of SO2 is limited by the acidity of the reaction products, as this oxidation route is efficient only near neutral conditions (Wilson et al., 1972). Further discussion on the variation of  $PM_{2.5}$ , its constituents, and gaseous pollutants is presented in SI section S3.1.

# 3.1. Source apportionment of elemental $PM_{2.5}$ (measured using Xact 625i)

The elements measured using the Xact 625i were subjected to source apportionment using PMF. The input dataset was found to be best represented by a seven factor solution namely, vehicular emissions, biomass burning, secondary chloride, Zn-K-Br rich, dust related, power plants and local coal combustion. As discussed in supplementary information section S2.1, measurements corresponding to only 16 elements out of the 36 elements measured by the Xact, were utilized for input to the elemental source apportionment (SA). It is important to note while the considered elements along with the organic and black carbon measurements present closure to total PM2.5 (SI S1), the limited no. of elements may limit our understanding of some of the sources resolved by elemental SA. Sources like secondary chloride are dominated solely by chlorine, while in case of the Zn-K-Br rich source, none of the dominant species point towards a specific emissions source. A greater number of elemental measurements in the future may add more meaning to the sources resolved in this study, by providing additional tracers. Also, it could potentially aid in further resolving factors like the Zn-K-Br rich factor taking advantage of more marker species. The sources corresponding to the apportioned factors were assessed based on the species dominating every factor profile. Each of the species was quantified in two ways:

- a) Based on the percentage of factor mass, given by the average concentration of the species of interest divided by the sum of the average concentration of each species within the factor
- b) Based on percentage species across factors, given by the concentration of the species of interest in the factor under consideration divided by the sum of the concentration of the same species across all factors

A detailed description of the resolved seven-factor solution (Fig. 2) is as follows:

# 3.1.1. Vehicular emissions

The vehicular emissions factor (Fig. 2(a)) was found to be dominated by S (36%) in terms of the % factor mass, followed by Cl (19%), K (17%), Fe (13%), Ca (7%) and Zn (6%) respectively in terms of the percentage factor mass. However, in terms of the percentage species across factors, vehicular emissions accounted for 60% of the total Mn content, followed by 33% of Ba, 30% of V, 22% of Zn, 15% of Ca, 13% of K, and 11% of S.

Sulfur and Vanadium is known to occur naturally in crude oil; while pollution control measures have remained focused on reducing sulfur content in fuels, studies have pointed out the use of sulfur in engine oil anti-wear additives (Fitch, 2019). Multiple studies in the past have attributed Mn, Fe, Zn, and Ba to vehicular emissions, brake wear, and engine wear, in particular, recognizing them as abundant trace elements in brake pads and brake lining (Gianini et al., 2012; Grigoratos and Martini, 2015; Rai et al., 2020b; Thorpe and Harrison, 2008). Ti and V have also been attributed to brake and tire wear in some studies in the past (Gerlofs-Nijland et al., 2019). Potassium is noted to be used as an anti-freeze inhibitor and as an additive in engine oils. Also, K is known to be present in all unleaded fuels (Spencer et al., 2006). Calcium and Chlorine are known to be added to engine lubricants, Ca-compounds serves as a base to neutralize acids, while Cl-based additives act as dispersants to retain dirt in suspension, to protect the engine (Dyke et al., 2007; Lyyränen et al., 1999; Rudnick, 2017).

In terms of the time variation (Figure S3(a)), this factor is significantly affected by the lockdown with a 96% reduction in average concentration from PLD to eLD-1 (Figure S6(b)), the time series, and the composition pie-chart (Fig. 2(b)) show a steady rise in the concentration

of this factor, while the factor concentration in phase-4 remains 70% lower than its pre-lockdown value.

As an additional proxy, mobility trends (Google LLC, 2020) (Fig. 2 (c)) quantifying the percentage change in transit station mobility w.r.t PLD, was compared with the time variation of this factor, and a significant correlation (Pearson R=0.81) between the two was noted.

In addition to the characteristic species noted above, this factor displayed a sharp diurnal peak coinciding with the morning rush hour and evening rush hour (Figure S4) during PLD and LD-4, when there was comparatively normal traffic load. During eLD-1 to LD-3, the vehicular movement has remained extremely restricted; thus, no diurnality in traffic-related emissions was found.

### 3.1.2. Biomass burning

In terms of the % factor mass, the biomass burning factor (Fig. 2(a)) was dominated by K (36%), followed by S (27%), Cl (21%), and Si (12%), respectively. Looking into the percentage species across factors, biomass burning was found accountable for 75% of the total Se content, followed by 58% of K, 19% of Si, and 14% of S.

Multiple studies across the globe have proposed the use of potassium as an elemental marker to identify biomass source profiles (Khare and Baruah, 2010; Pant and Harrison, 2012; Reche et al., 2012; Shridhar et al., 2010). Past studies have also reported Se to reach significant levels in biomass grown in selenium-rich soils (Goldstein, 2018), which in turn are common in northern India (Sharma et al., 2009). Silicon is known to be emitted from the pyrolysis of fibers in biomass like straw, cereal, and grass (Obernberger et al., 2006). Li et al. (2003) concluded that for fresh biomass burning plumes, most potassium exists as KCl, while in aged plumes, the chlorides are partly replaced by sulfates—thus providing evidence for high sulfur and chloride concentrations in conjunction with potassium in biomass associated source inventories.

The average factor concentration is found to lower by 25% in eLD-1 (Figure S6(b)); however, that may be a direct consequence of lower biomass burning emissions. Again it is not instinctive to assume any strong dependence of the lockdown event over biomass burning emissions. Thus it is difficult to ascertain whether the decrease in the concentration stemmed from the lockdown. The concentration starts increasing in April and peaks in May, which also coincides with the wheat harvesting season, thus resulting in increased residual crop burning activities (Jethva et al., 2019). The factor time series was also compared with satellite-based fire counts (LANCE FIRMS, 2020) in a 200 km radius of the sampling site (Fig. 2(d)), and a significant correlation (Pearson R = 0.71) was observed between them.

# 3.1.3. Secondary chloride

The Secondary Chloride factor (Fig. 2(a)) is solely dominated by chlorine in terms of factor mass, with Cl accounting for 98% of the factor mass. Also, in terms of % species across factors, secondary chloride contributes to 89% of total measured Cl and 27% of total Br.

The diurnal variation associated with this factor (Figure S4) is very similar to that of  $NH_4$ , with a sharp peak around 6:00 IST. This leads us to the possibility of this factor stemming from ammonium chloride. With lower saturation vapor pressure, ambient ammonia and HCl may condense in the particulate phase and vaporize back with an increase in saturation vapor pressure after sunrise.

A similar factor from source apportionment of  $PM_1$  in Delhi was observed by Jaiprakash et al. (2017). It was suggested that HCl fumes transported from metal processing plants to the north-west of Delhi reacted with the high ammonia concentrations in Delhi to condense in the particulate phase (Warner et al., 2017). Similar conclusions were reached upon by Gani et al. (2019) for the high particulate chloride concentrations observed by them.

The secondary chloride factor seems to have no dependence on the lockdown event as the average concentration of this factor increases marginally from PLD to eLD-1  $(3.94-4 \,\mu\text{g/m}^3)$  (Fig. 2(b)).

From Figure S3(a), secondary chloride time series, we can note that

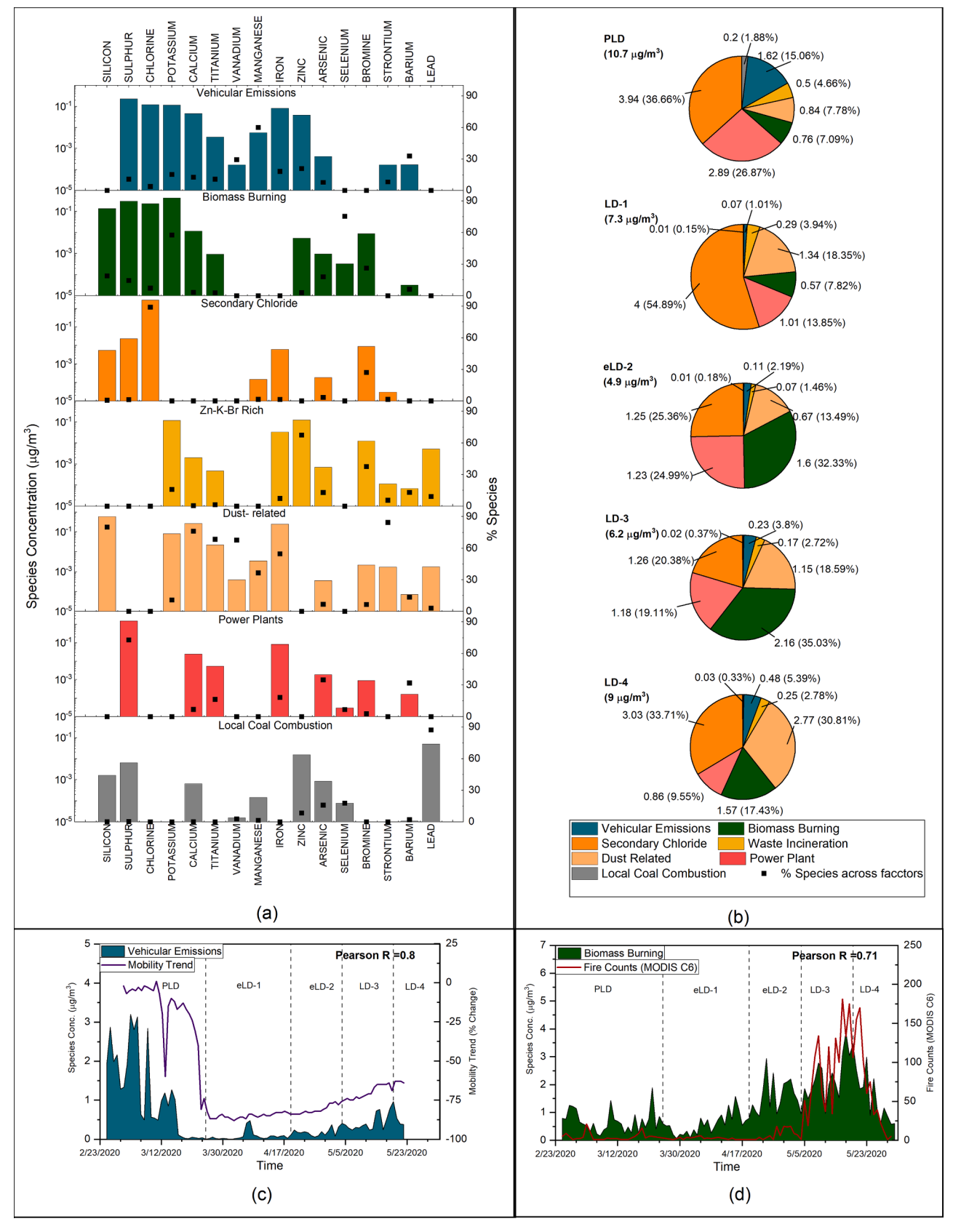


Fig. 2. Source apportionment results for elemental particulate matter: (a) resolved source/factor profiles; (b) phase-wise contribution of each factor to total elemental fraction of PM<sub>2.5</sub>; (c) Correlation of vehicular emissions with mobility trends (d) Correlation of biomass burning with fire counts.

almost all peaks for this factor correspond to a local wind direction in the sector of  $302\text{--}333^\circ$  or NW direction. Also, the factor concertation is found to decrease noticeably in eLD-2 ( $1.25~\mu\text{g/m}^3$ ) and remain low in LD-3 ( $1.26~\mu\text{g/m}^3$ ) (Fig. 2(b)). This again seems to have a dependence on the wind direction, starting from the beginning of eLD-2 up till the middle of LD-3, a shift in wind direction towards the southeast can be noted. However, the wind direction again shifts to the northwest towards the end of phase-3, which marks the rise in the secondary chloride concentrations again. In addition to the dependence on wind direction the reduction in average particulate-bound chlorine concentrations from PLD to LD-3 ( $3.94\text{--}1.26~\mu\text{g/m}^3$ ), is also influenced by the rising ambient temperatures during the summer months (Figure S2), this is in line with the observations of past studies assessing the chloride levels in Delhi. (Gani et al., 2019; Rai et al., 2020a).

It is important to take note that the diurnal behavior associated with this source (Figure S4), reassures the existence of chlorine in form of NH<sub>4</sub>Cl. Also, the dependence of this factor on the north-westerly winds as observed in this study, lend further support to the potential role of HCl fumes emitted in the north-west, neutralized by the high NH $_3$  levels in Delhi, as proposed by Jaiprakash et al., (2017). The possible sources of Cl or Br emissions may include a variety of sources like waste burning or industries; however, to account for the lack of dependence of this factor on the lockdown and following relaxations, the source of HCl/HBr must also remain unaffected/minimally affected by the lockdown.

### 3.1.4. Zn-K-Br rich

In terms of % factor mass, this factor is mainly composed of Zn (42%), K (40%), and Fe (11%). However, in terms of % species across factors, these factors contribute to 68% of total Zn, 38% of total Br, and 16% of K (Fig. 2(a)).

Multiple studies in the past have attributed a Zn-dominated factor to waste incineration (Gupta et al., 2012; Julander et al., 2014; Parekh et al., 1967; Sweet et al., 1993). These studies have mainly been associated with electronic or municipal waste burning, where a halide catalyzes the volatilization of metals to form metal halogenides, usual metals related to waste incineration in addition to Zn, include K, As, Fe, and Pb. While Cl is a more abundant halide, but Vehlow et al. (2003) have discussed how Br may be high in plastics containing flame retardants and, in turn, drive the volatilization of heavy metals like Zn Fe and As. However, Zn and As have also been attributed to iron/steel industries and waste incineration (Duan and Tan, 2013). Also, past studies have attributed Zn-Pb-Cl to industrial emissions (Bullock and Gregory, 1991).

This ambiguity in the published literature regarding tracer for waste incineration/industrial activities has lead us to define this factor as a Zn-K-Br rich factor only. In terms of the time variation (Figure S3(a)) the factor in line with total PM<sub>2.5</sub> decreases by 42% in eLD-1 w.r.t prelockdown, followed by 85%, 54%, and 50% in each of eLD-2 to LD-4 w.r.t PLD concentrations (Figure S6(b)).

# 3.1.5. Dust related

The predicted dust-related source profile (Fig. 2(a)) is dominated by Si, accounting for 48% of the factor mass, followed by 22% and 20% of the factor mass for Ca and Fe, respectively. In terms of % species across factors, dust-related source accounts for 84% of total Sr, 80% of total Si, 76% of Ca, 68% each of Ti and V, 55% of Fe, and 37% of Mn. Each of the above-noted species has been extensively used as tracers for road dust/crustal elements in multiple studies across the globe (Gupta et al., 2007; Kothai et al., 2011; Rai et al., 2020a; Sharma et al., 2016; Sun et al., 2019).

In terms of the time variation (Figure S3(a)) of this factor, there seems to be no observable effect of the lockdown on dust-related particulate matter. However, we observe a significant correlation of the factor concentration with ambient temperature (Pearson R=0.64) (Figure S2(a)) and an inverse correlation with RH (Pearson R=-0.67) (Figure S2(a)), which is in agreement with several past studies (Csavina

et al., 2014; Jayamurugan et al., 2013). Also, during LD-4, we observe an increase in the average concentration of this factor, from 1.15  $\mu$ g/m³ in LD-3 to 2.77  $\mu$ g/m³ in LD-4 (Fig. 2(b)), which may be influenced by multiple meteorological parameters like WD, WS or gust events.

# 3.1.6. Power plants

Considering the % factor mass, sulfur solely dominates this factor profile accounting for 93% of the total factor mass. In terms of the % species across the factors, the power plants factor contributes to 73% of the total sulfur, 35% of As, and 32% of total Ba (Fig. 2(a)).

In this study, the power plants factor (Figure S3(a)) displays a significant correlation with the SOR (Fig. 1(d)) (Pearson R=0.922), signaling towards the sulfur content in the particulate phase is actually in the form of aqueous sulfate. Also, past studies evaluating power plant emissions as well as source apportionment studies have highlighted the use of As and Ba as tracers for coal-based power plant emissions (Reddy et al., 2005; Zhao et al., 2017; Zoller et al., 1974).

Observing the time series of this factor, we do note a 65% decrease in eLD-1 w.r.t the PLD concentrations (Figure S6(b)). A recent report from the Power System Operation Corporation (POSOCO, 2020) does indicate a significant reduction (44% reduction in April compared to last year) in the power demand due to the closure or scaled-down operations in almost all industries due to the lockdown, which in turn could lead to temporarily scaled down operations at some power plants. Thus, some order of reduction in source emission can also be partially responsible for the significant drop observed in the factor concentration at the receptor.

However, it would be implausible to attribute the entire reduction to the lockdown alone, as there has been significant variation in the factor concentration within the PLD (-54% to +89% w.r.t PLD average) (Figure S6(b)), indicating some role of meteorological or other transport variables rather than the source emission alone for the variation in the concentration. Again, during eLD-2, the average concentration is found to increase relative to PLD levels; however, the concentration again starts to fall during LD-3 and LD-4, thus advising of some external metrological/transport phenomena affecting the concentration values.

#### 3.1.7. Local coal combustion

The coal combustion factor (Fig. 2(a)) is dominated by Lead, Zinc, and Sulfur accounting for 66%, 21%, and 8.5% of the total factor mass, respectively. Considering the % Species across factors, coal combustion is responsible for 87% of Pb, 18% of Se, 16% of As, and 9% of Zn. While coal combustion is found to account for only 0.3% of total sulfur, it is essential to note that the % contribution of this factor to elemental PM $_{2.5}$  has remained quite low (less than 1.9%) throughout the study period.

As and Se have been widely used as markers for coal combustion (Gupta et al., 2007; Hien et al., 2001; Lee et al., 2008; Sharma et al., 2007). Zn again has been used as a marker for coal combustion in India due to relatively higher Zn content in Indian coals (Almeida et al., 2006). While commercially available coal has lower Pb content, Negi et al. (1967) reported the higher concentrations of Pb and Zn in domestic soft coal. It is also important to note that domestic Indian coals have been found to have low sulfur content (less than 0.6% by mass), with an exception to coal deposits in north-eastern India with high sulfur content (Chandra and Chandra, 2004; Sarkar, 2009). Also, past studies have reported Indian power plants to utilize blends of imported and domestic coals supporting the higher sulfate emissions from power plants (Central Electricity Authority, 2012; Chandra and Chandra, 2004).

Evaluating the temporal variation associated with this factor (Figure S3(a)), we notice that the lockdown implementation brings about a 95% reduction in the average concentration of the coal combustion source, comparing eLD-1 to PLD conditions. With increasing relaxations, the percentage reduction in average concentration w.r.t the PLD falls to 90% in eLD-2 and LD-3 and finally 85% in LD-4 (Figure S6 (b)).

Since the source profiles and supporting literature indicate domestic

soft coal burning, the real-world sources may be connected to small scale industrial setups, eateries, or household usage of domestic grade coal, and such sources appear to be drastically affected by the lockdown and display only a marginal increase in emissions even with increasing relaxations. Such a variation could possibly stem from the massive outflow of migrant laborers from the NCT region, resulting in the sudden downfall of domestic coal usage for cooking purposes (Roy and Agarwal, 2020).

# 3.2. Source apportionment of organic aerosols (measured using Q-ACSM)

The organic content of the total  $PM_{2.5}$  mass is subjected to source apportionment using PMF. A six-factor solution was found to fit the input data best. The apportioned factors were identified by the mass spectra signatures, their correlation with tracers, and their diurnal behavior (Ulbrich et al., 2009; Zhang et al., 2005b). The present study further correlates each apportioned factor to corresponding reference factor profiles from Ng et al. (2011). Fig. 3 presents the predicted mass spectra for each profile, along with their temporal variation and correlation with external markers. The detailed description of each predicted source profile is as follows:

#### 3.2.1. Semi-volatile oxygenated organic aerosol (SVOOA)

The factor profile, as seen in Fig. 3(a), is characterized by a significant peak at m/z 43, which is a characteristic of less oxidized secondary organic aerosol (Li et al., 2019; Zhu et al., 2018). The diurnal variation (Figure S5) of this factor presents two peaks: early morning (6:00 – 9:00 IST) and a weaker peak at midnight, signaling SVOOA concentrations to be affected by photo-oxidation of fresh emissions (morning peak) along with boundary layer height (midnight peak), similar to observations made by Chakraborty et al. (2018). The SVOOA source profile predicted from the PMF analysis was noted to have a Pearson R correlation of 0.93 with the reference SVOOA profile from Ng et al. (2011)

The SVOOA factor time series displayed a strong correlation with NO $_3$  (measured using ACSM) (Pearson R = 0.95) (Fig. 3(c)), which is in agreement with the trend reported in past studies (DeCarlo et al., 2010; Dzepina et al., 2009; Volkamer et al., 2006), and is attributed to the analogous semi-volatility of SVOOA and nitrate resulting in similar gasparticle partitioning.

The SVOOA factor drops significantly (86%) after the lockdown is implemented; the emissions increase with increased relaxations from eLD-2 to LD-3; however, there is a small drop (18%) in average concentration again from LD-3 to LD-4 (Figure S6(c)).

# 3.2.2. Hydrocarbon-like organic aerosol (HOA)

Alkyl fragment signatures distinctly mark this factor profile (Fig. 3 (a)) with prominent contributions from m/z 55 and 57 (Aiken et al., 2009; Ng et al., 2011). The resultant HOA profile has a strong correlation (Pearson R = 0.95) with reference HOA spectra from Ng et al. (2011).

Past studies have found HOA to correlate well with black carbon (BC) (Mohr et al., 2009; Sun et al., 2016). In the present study, we note an excellent correlation between BC and HOA (Pearson R = 0.96) (Fig. 3 (c)) during the PLD phase; however, post-lockdown, the trend of BC and HOA become completely disparate, resulting in a negligible correlation between the two. The significant correlation with BC often is taken as support for the vehicular origin of HOA (DeWitt et al., 2015).

However, from section 3.1.1, we note the vehicular emissions to drop significantly post-lockdown (96%) while HOA concentrations lower only by 14% post-lockdown. At the same time, it departs from the trend followed by BC (Fig. 2(d)), indicating that during the lockdown, HOA originates from a source other than vehicular emissions. This uncharacteristic loss of correlation with BC and the potential sources supplementing HOA during the lockdown will be investigated further in section 3.3.

The initial studies that looked into the deconvolution of HOA from POA (Zhang et al., 2005a) suggested its connection to vehicular origin

based on the significant correlation with vehicular markers like  $NO_x$  and BC and the fine mode of particulate matter corresponding m/z 55 and 57 as compared to m/z 44 which grows larger while aging. Zhang et al. (2005a) also discussed car-chaser and lab-based studies, wherein both diesel emissions and lubricant combustion resulted in HOA like spectra, as heavy oils, lubricants, cooking oils are known to correspond to m/z 55, while mass spectra associated with gasoline and diesel-like fuels displayed a more definite m/z 57 peaks.

Hao et al. (2014) also observed appreciable HOA contributions in a low-traffic village setting. They attributed the source to be a combination of industrial, cooking, and biomass burning along with the low contribution from traffic.

Thus, it may be hypothesized that either HOA during the lockdown originates from diesel/lubricant based emissions from sources other than vehicles, like diesel-based generators in industries or cooking-related activities. However, similar to SVOOA, even HOA experiences a sharp reduction towards the end of LD-4. The potential causes of this erratic behavior would be investigated further in section 3.3.

# 3.2.3. Biomass burning organic aerosol (BBOA-1 and BBOA-2)

In the present study, we resolve two separate biomass burning related factors (Fig. 3(a)). However, BBOA-1 can be categorized as a fresh/ primary emission, with its mass spectra highly correlated to the BBOA profile from Ng et al. (2011) (Pearson R = 0.937). For the other BBOA profile, i.e., BBOA-2, we observe enhanced concentrations of m/z43 and m/z44, indicating that BBOA-2 is relatively aged. Also, the diurnal variation (Figure S5) associated with BBOA-1 displays primary emission like behavior, with early morning peaks, while BBOA-2 also displays peaks around noon, which is a characteristic of m/z44 or  $\mathrm{CO}_2^+$ , indicating the possibility of regionally transported emissions responsible for BBOA-2.

BBOA-2 also shares a good correlation with the Ng et al. (2011) reference BBOA profile (Pearson R = 0.82). Both BBOA-1 and BBOA-2 are marked by intensified peaks corresponding to m/z 60. Levoglucosan is known to be proportional to  $C_2H_4O_2^+$  (a fragment at m/z 60) is extensively used as a marker for biomass burning in AMS-based studies (Aiken et al., 2009).

It is also important to note that while both the BBOA factors present a good correlation with the reference BBOA profiles, these factors profiles do share similarities with Coal Combustion Organic Aerosol (CCOA) detected by multiple studies in the past (Huang et al., 2014; Zhu et al., 2018). However, resolving the CCOA profile during ambient sampling is often contingent upon tracer fragments like PAHs and C<sub>6</sub>H<sub>10</sub>O<sup>+</sup> and heavier m/z's (Lin et al., 2017), which can be measured using the HR-ToF-AMS or ToF-ACSM. Since, the present study utilizes a q-ACSM limiting the m/z spectra to 120, the BBOA factors may have a trace or high contributions from CCOA factor that cannot be resolved with certainty with the single PMF due to lack of tracer ions. Past studies have also noted that splitting of factors, in absence of strong tracers, is most likely a mathematical artifact rather than a true component (Ulbrich et al., 2009). Nevertheless, the potential association of the BBOA factors with coal combustion or related activities, is further investigated in section 3.3 using double PMF and elemental tracers.

Similar to the biomass burning factor in section 3.1, it is not intuitive to presume an effect of the lockdown on biomass burning. However, comparing the two BBOA factors, we see that BBOA-1 displays higher concentrations in pre-lockdown, while reduced order (76%) values following lockdown steadily rise from eLD-1 to LD-3. BBOA-2 displays lower concentrations in the PLD period and steadily rise to a maxima (5.1  $\mu$ g/m³) up till LD-3 (Fig. 3(b)). Thus, indicating that while the lockdown leads to a decrease in the primary BBOA emissions (BBOA-1), it in some way enhances the regional transported/aged fraction of BBOA (BBOA-2). However, similar to both SVOOA and HOA, both BBOA factors significantly reduce both in absolute concentration and percentage contribution in LD-4 (Figure S3(b) & Fig. 3(b)).

Interestingly none of the BBOA factors display any positive

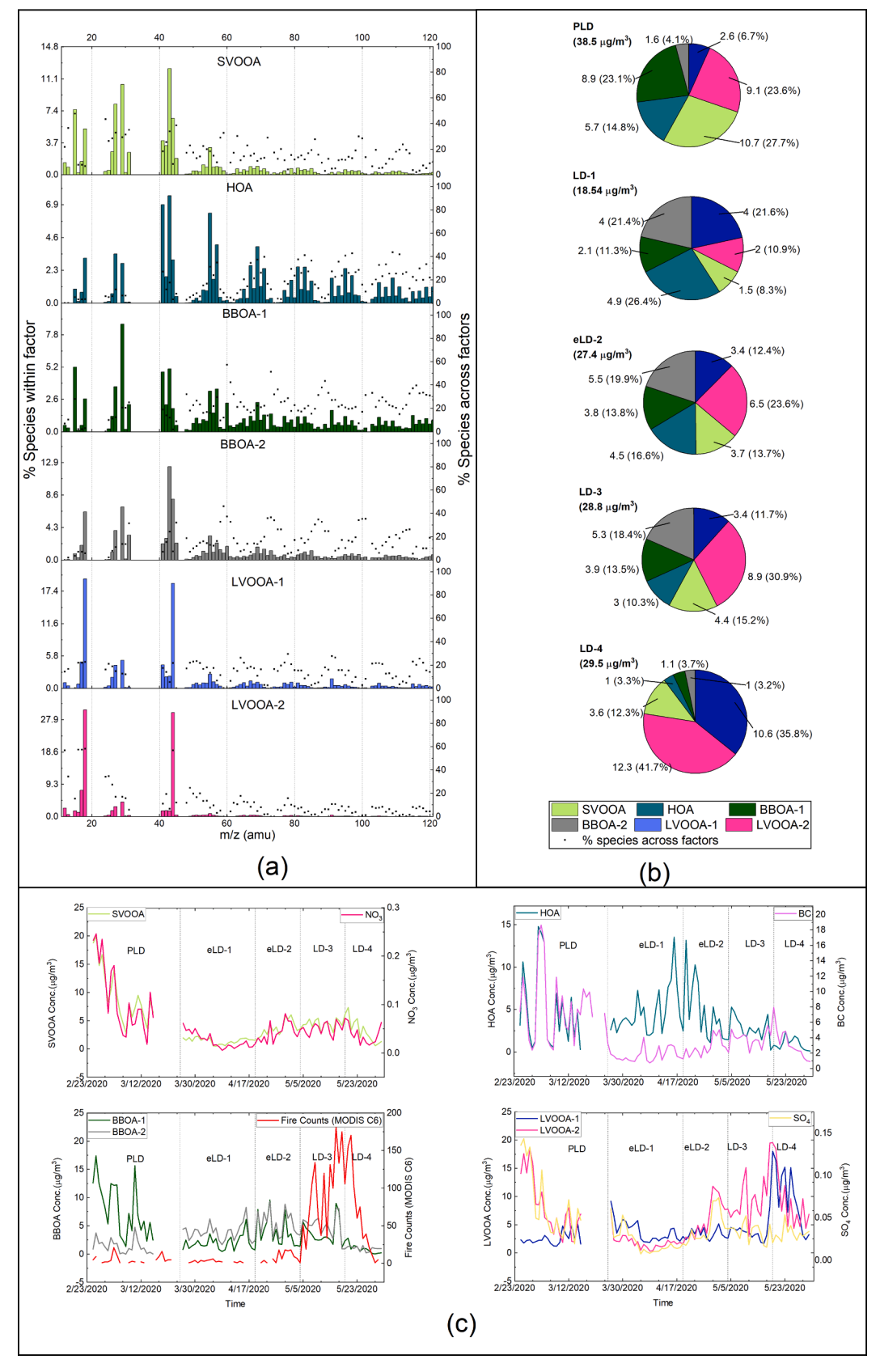


Fig. 3. Source apportionment results for organic particulate matter: (a) resolved source/factor profiles; (b) phase-wise contribution of each factor to total organic aerosol; (c) correlation of factors with external markers.

correlation or similar trend with the satellite-based fire counts (LANCE FIRMS, 2020) (Fig. 3(c)), which was seen in the potassium dominated biomass burning factor in section 3.1 and neither with the biomass burning factor resolved from elemental SA.

A potential contributing factor to this discrepancy may stem from the stance that the tracers used to resolve these factors, i.e., m/z 60 and  $K^+$ , point to different types of combustion processes. A study by Brown et al. (2016) presented a comparison between different biomass burning markers like  $K^+$ , BC, and levoglucosan or, in turn m/z 60. It was noted that  $K^+$  and BC are more prominent products in flaming combustion (which is usually captured as fire counts). However, levoglucosan is a more prominent emission in the case of smoldering combustion (Lee et al., 2010).

Another probable cause may be that BBOA emissions can be associated with multiple sources and may not yield a good correlation with a single  $\rm K^+$  resolved biomass burning source alone, rather a combination of sources. This possibility is investigated further in section 3.3.

3.2.4. Low volatile oxygenated organic aerosol (LVOOA-1 and LVOOA-2) LVOOA is addressed as an aged or oxidized aerosol and is majorly marked by a distinct peak of m/z 44 or CO $_2^+$ . In this study, we resolve two LVOOA factors (Fig. 3(a)), i.e., LVOOA-1 and LVOOA-2. Both the LVOOA factors display a strong correlation with the Ng et al. (2011) reference spectra (Pearson R = 0.95, 0.93 for LVOOA-1, and LVOOA-2, respectively)

Observing the temporal variation, we see that LVOOA-2 is at a high concentration (9.1  $\mu g/m^3$ ), which reduces after the lockdown (2  $\mu g/m^3$ ) and steadily rises to a noticeably high concentration in LD-4 (12.3  $\mu g/m^3$ ). On the other hand, LVOOA-1 mostly remains at a lower concentration from PLD to LD-3 (from 2  $\mu g/m^3$  to 4  $\mu g/m^3$ ); however, it rises to a significant concentration in LD-4 (10.6  $\mu g/m^3$ ) (Fig. 3(b)). It is important to note that all apportioned organic factors decrease considerably in LD-4, while both the LVOOA factors experience a significant rise

LVOOA is known to correlate well with sulfate, citing the similar low-volatility observed in both species (Zhu et al., 2018). In Fig. 3(c), we see that LVOOA-1 neither follows the trend nor is correlated to sulfate, whereas LVOOA-2 expresses a significant correlation with sulfate (measured using ACSM) during PLD (Pearson R = 0.93) and continues to display a significant correlation up till LD-2 (Pearson R = 0.75); however, the correlation significantly deteriorates in LD-4. The decreased correlation with sulfate may point towards a change in source contributing to LVOOA-2 in LD-4, which will be investigated further in section  $^{3}$  3

Investigating the diurnal variations associated with both factors (Figure S5), we see that LVOOA-2 displays a flat diurnal profile with a marginal peak at noon, which is characteristic of CO<sub>2</sub><sup>+</sup> formation by photochemical oxidation. However, if we look at the phase-wise diurnal variation, the diurnal profile for LVOOA-1 in lockdown phase-4 behaves like a primary pollutant diurnal with an early morning peak rather than the afternoon peak, suggesting a primary aerosol-like formation mechanism for LVOOA-1.

Earlier in section 3, we noted low SOR and NOR values, which usually correspond to primary rather than secondary aerosols. We must also take into account that LD-4 began right after the period when ozone had reached its peak concentrations (section 3.1.2).

All these facts taken collectively indicate that in some way, all primary and intermediate organic aerosols are chemically aged in the presence of high  $O_3$  to form LVOOA, leading to a reduction in all other organic factors and a significant rise in LVOOA. Jimenez et al. (2009), on a similar note, stated that the atmospheric oxidation of organic aerosol (OA) converges to LVOOA regardless of the original OA source. However, it is also important to note that the diurnal variation of LVOOA-1 hinted towards its primary emissions. Another study by Liggio and Li (2013) suggested a mechanism for the formation of oxygenated primary organic aerosols by uptake of primary oxygenated organic gases to

aerosols, and thus presents a possible explanation for the primary rather than secondary origin of LVOOA-1.

# 3.3. Combined source apportionment of elemental $PM_{2.5}$ , black carbon, and organic $PM_{2.5}$

In this section, we further resolve the sources of organic aerosols and interpret them better using elemental markers measured using the Xact 625i. We subject the elemental PM<sub>2.5</sub> and black carbon measurements from the Xact 625i and Aethalometer, respectively, along with the organic aerosol factors resolved in section 3.2, to source apportionment using PMF. As discussed in section 2.2 and in further detail in SI section S2.1.1, our efforts build upon the work of Petit et al., (2014), which introduced the double PMF methodology initially. While sections 3.1 and 3.2 have elucidated the impact of the lockdown on the elemental and organic fragments of PM<sub>2.5</sub> separately, this section gives a broader picture of the impact of the lockdown on sources encompassing both the organic and elemental fragments of  $PM_{2.5}$  along with black carbon. This section also bridges the organic aerosol factors apportioned in section 3.2 to more realistic real-world sources, using elemental tracers. The implementation of the double-PMF is discussed in SI S2.2 and in greater detail in Petit et al., (2014)

The double-PMF analysis results in nine source profiles, i.e., vehicular emissions, biomass burning, secondary chloride, Zn-K-Br rich, dustrelated, power plant, local coal combustion, combustibles factor (CF-1), and LVOOA dominated that is found to best explain the variability of the input dataset. The results of the double-PMF analysis are presented in Fig. 4; the resolved source profiles as seen in Fig. 4(a) highlight the fact that seven (vehicular emissions, biomass burning, secondary chloride, Zn-K-Br rich, dust-related, power plant, local coal combustion) out of the nine resolved factors are extremely similar to the 7-factor solution resolved from the elemental source apportionment in section 3.1. The elemental fraction of the double-PMF resolved sources are found to have an appreciable correlation (Pearson R > 0.9) with their counterparts in the elemental-PMF sources, and the same has been utilized to name the double PMF factors. The remaining two factors are dominated by the factors resolved in organic source apportionment instead of the elemental tracers and are named accordingly.

# 3.3.1. Vehicular emissions

In addition to being marked by high concentrations of S, K, Fe, and tracers like Mn and Zn, as seen in the elemental SA factor, the double PMF apportions 35% HOA, 33% BC, and 18% SVOOA to vehicular emissions. As discussed in section 3.2.2, the temporal variation of HOA was well correlated with BC during PLD but deviated from the trend followed by BC post-lockdown. The temporal variation of vehicular emissions source (Fig. 4(b)) and the fractional contribution of the vehicular emissions source to the BC and HOA time variation (Fig. 4(c)) supports the vehicular origin of HOA and BC during PLD and LD-4, thus explaining the good correlation during those periods and also justifying the observed loss of correlation, from eLD-1 to LD-3 when the vehicular emissions fall down and no longer remain a major contributor to BC or HOA.

#### 3.3.2. Biomass burning

In line with its counterpart resolved through elemental source apportionment discussed in section 3.1.2, the double PMF resolved biomass burning source is marked by the high levels of K, S, Cl, and Se. Considering the organic SA factors, 40% of LVOOA-2, 35% of BBOA-2, 19% of BC, and 11% of SVOOA have been apportioned to the biomass burning source. As discussed in section 3.2.4, both apportioned LVOOA factors were found to increase in LD-4, which in turn also saw a rise in fire counts and biomass burning factor resolved by the elemental SA. A substantial part (40%) of LVOOA-2 being apportioned to double PMF biomass burning factor highlights the contribution of the biomass burning related activities in the rise of LVOOA-2 during LD-4. This

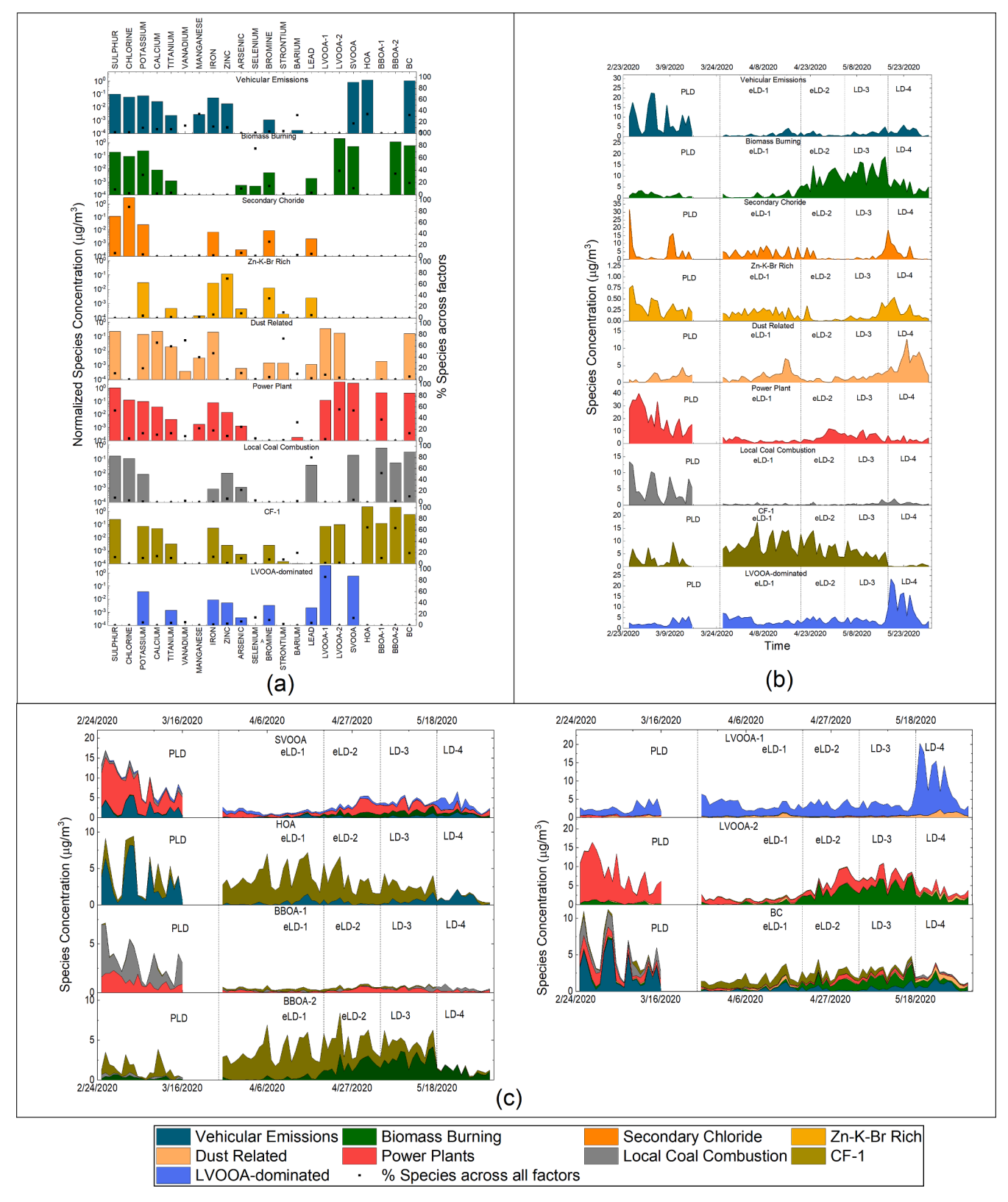


Fig. 4. Organic-Inorganic coupled source apportionment: (a) resolved source/factor profiles; (b) temporal variation of each resolved factor; (c) fractional contribution of each double PMF resolved factor to organic SA factors and black carbon.

impact can be clearly observed in Figure (4(c)), where biomass burning emissions are the major contributor towards LVOOA-2 during LD-3 and LD-4. It is also interesting to take note that while the BBOA-2 factor as a whole didn't present an appreciable correlation to elemental SA biomass

burning factor, the double PMF connects the biomass burning activities marked by potassium tracers to contribute to a significant fraction, i.e., 35% of relatively aged BBOA or BBOA-2 on an average and can be clearly seen to dominate the BBOA-2 temporal variation during LD-3

#### and LD-4 (Fig. 4(c)).

Secondary Chloride and the Zn-K-Br Rich factor, while are well correlated with their counterparts resolved with the elemental SA, both in terms of the source profile and temporal variation, double PMF attributes none of the organic emissions to these factors. This may be due to the unlikely event that these sources are not responsible for any organic emissions, or the tracers are impacted by some meteorological conditions or chemical transformations, rendering them unable to resolve the associated organic fragments. Thus, their source profile and temporal variation can be completely explained by their counterparts resolved by elemental SA discusses in section 3.1.3 and 3.1.4, respectively.

The *Dust Related factor*, similar to the secondary chloride and Zn-K-Br rich factors, doesn't contribute substantially to the organic fraction of  $PM_{2.5}$ . The double PMF does highlight some minor contributions (<5% of species sum) of this source to LVOOA, BC, and BBOA-1; however, these contributions may result from contaminants common to dust-related sources, as discussed by, due to their interaction with multiple emission sources resulting in deposition of contaminants on dust-related PM.

#### 3.3.3. Power plant

As discussed for the elemental SA in section 3.1.6, in case of the double PMF resolved power plants factor too is marked by S, As, and Ba. However, it is interesting to note that that the power plant factor accounts for 56% of LVOOA-2, 54% of SVOOA, 38% of BBOA-1, and 13% of BC. As discussed in section 3.1.6, the sulfur content measured is mostly in the form of sulfate, which in turn is found to correlate well with LVOOA-2 up to LD-3, as discussed in section 3.2.4 (Fig. 3(c)). The fractional contribution of this source to LVOOA-2 (Fig. 4(c)) demonstrates that the power-plant emissions contribute significantly to total LVOOA-2 levels up to LD-2 (after which biomass burning dominates), justifying the appreciable correction of sulfate and LVOOA-2 up till LD-2 and its deterioration thereafter. It is also interesting to note that the power plant source, while being responsible for a significant amount of LVOOA-2, which is usually associated with regionally transported of aged OA, is also found to contribute to around 54% of SVOOA, which is more often linked with local, or moderately aged OA. The authors feel further investigation through back trajectory analysis may aid in understanding the origin of these source emissions to help understand the reason behind its significant contribution to both LVOOA-2 and SVOOA.

As discussed in section 3.2.3, the inability of the ACSM to measure higher m/z fragments, especially PAHs, renders the PMF solution unable to resolve the CCOA or COA with certainty. The power plant emissions contributing to the BBOA-1 levels (Fig. 4(c)) indicates the possibility of BBOA-1 having a coal combustion related origin.

#### 3.3.4. Local coal combustion

Similar to the elemental SA (section 3.1.7), the coupled SA coal combustion factor is dominated by Pb, accounting for more than 80% of total Pb. In terms of the organic content, the double PMF accounts for this factor to contribute to 52% of the total BBOA-1on average (Fig. 4 (a)). The presence of BBOA-1 in the power plants factor discussed earlier indicated the possibility of CCOA origin of BBOA-1; the presence of BBOA-1 in the coal combustion factor further reinforces this hypothesis that BBOA-1 has a coal combustion related origin. The same can be reaffirmed through the high fractional contribution of the local coal combustion factor to the BBOA-1 levels (Fig. 4(c)). This observation also highlights another advantage of double PMF as being used to better resolved or identify ACSM based organic sources, even when other organic tracers are missing. Other than BBOA-1, 10% of total BC is also attributed to the local coal combustion source.

#### 3.3.5. Combustibles factor-1

As discussed earlier, unlike the other coupled SA sources, the CF-1 and LVOOA-dominated sources are marked by organic SA factors as

tracers rather than the elemental markers. The CF-1 factor contributes to 65% of HOA and 64% BBOA-2 along with 19% of BC, and 12% of S. The BC and sulfur content indicate some form of combustion, while both HOA and BBOA-2 signal towards the primary nature of the emissions associated with this source. The fractional contribution of the CF-1 source (Fig. 4(c)) to various coupled factors indicates that the CF-1 source supplemented the HOA resolved from organic SA during the lockdown, which prevented HOA from reducing sharply with plummeting vehicular emissions. Based on the fractional contribution of these sources to BBOA-2 (Fig. 4(c)), the CF-1 source dominates the BBOA-2 levels up till eLD-2. As discussed in sections 3.2.2 and 3.2.3, both HOA and BBOA-2 may be related to cooking activities, which implies that the CF-1 source emissions may stem from cooking activities, waste burning, or some other form of combustion activity, however, due to the lack of a reliable/ well-accepted marker to identify the actual source of this factor, we continue to refer to as an CF-1 source.

#### 3.3.6. LVOOA-dominated

Like the CF-1 factor, this factor is populated by organic markers and accounts for 87% of total LVOOA and 13% of SVOOA. Interestingly, the factor is independent of any elemental/organic factor except LVOOA-1. As discussed in section 3.2.4, LVOOA-1 displayed diurnal behavior similar to primary organic aerosols, and now the LVOOA-1 factor not considerably associating with any other organic or elemental marker as resolved by double PMF further supports the hypothesis of the increased  $\rm O_3$  levels giving rise to increased LVOOA-1 levels in LD-4.

In addition to further apportioning the organics PMF derived factors, the elemental tracers, also aid in apportioning black carbon to real world sources, via the double PMF. As discussed earlier in account of the double-PMF resolved vehicular emissions, the notable contribution of the vehicular emissions to BC and HOA during PLD and LD-4, allows us to interpret the good correlation between HOA and BC, during these periods and loss of correlation during other times. A recent work by Goel et al., (2021), discussed the variation of black carbon sources during the lockdown, utilizing the wavelength-based two-component Aethalometer model proposed by Sandradewi et al., (2008). The original work proposing double-PMF (Petit et al., 2014), too utilizes the Aethalometer model, derived sources as input to the second PMF, in the two staged double PMF. However, in case of the present study we note that the BC sources' time variation derived using the Aethalometer model were highly correlated with each other (Pearson R > 0.9). Since the PMF technique is limited in its ability to resolve highly correlated input data (Ulbrich et al., 2009), we use total BC as input to the double PMF rather than the Aethalometer model derived BC fractions. The authors believe the use of the elemental tracers in the double PMF methodology, allows for an independent method to apportion BC; however, the comparison of the results with those of the two-component model will prospectively be explored in future works.

### 4. Conclusions

The COVID-19 lockdown resulted in an unprecedented decline in anthropogenic activities, which in turn led to a considerable reduction ( $\sim$ 54%) in ambient PM<sub>2.5</sub> levels. The detailed source apportionment results presented in this study reveal the varying impact of the lockdown on different sources contributing to the elemental and organic fractions of PM<sub>2.5</sub>. Source apportionment of elemental PM<sub>2.5</sub> yielded seven source profiles; the vehicular emissions, coal combustion, and Zn-K-Br rich sources were severely impacted by the lockdown. However, the lockdown seemed to have minimal or no impact on biomass burning and dust-related sources. The dust-related factor displayed dependence on meteorological factors, while increased biomass burning emissions coincided with the crop burning season. The power plants-related elemental PM seems to be affected by both the lockdown and meteorological parameters. Interestingly, the secondary chloride factor observed elevated concentration peaks majorly from the north-west

direction and remained largely unaffected by the lockdown.

The organics-only PMF resulted in 6 factors, i.e., SVOOA, HOA, two BBOA, and two LVOOA factors. The lockdown seems to have an appreciable effect on SVOOA factor concentrations with a reduction (86%) in eLD-1, followed by increased concentrations with relaxations in the lockdown. The fresh BBOA emissions (BBOA-1) decline following the lockdown, while the aged BBOA emissions(BBOA-2) rise, signaling intensified transport of BBOA related emissions from regional sources following the lockdown. HOA concentrations were marginally affected by the lockdown indicating sources other than vehicular emissions played a dominant role in HOA related emissions, contrary to the belief of HOA being dominated by vehicular emissions. The organic aerosol (OA) source apportionment also highlights a sharp rise in the LVOOA concentrations in LD-4 accompanied by a concomitant decay in concentrations of all other resolved OA sources; this rise is attributed to the oxidation of primary OA due to high ozone concentrations.

The double PMF implemented in the present study enabled much better interpretation of the temporal variation of the organic sources resolved by the organic SA, and successfully connected the elemental SA and organic SA results to give a complete picture of the impact of the lockdown on total  $PM_{2.5}$  rather than just one the organic and inorganic fractions individually.

This is also the first study to quantify the impact of the COVID-induced lockdown on highly time-resolved sources of ambient  $PM_{2.5}$  in India. These results have important implications for guiding future policies targeted and decreasing PM levels in not only Delhi but the entire IGP so that the actions are targeted on actual sources of emission, knowing the level of impact a particular source has on total PM levels. The results also highlight a prime concern for driving future emission control strategies, especially upcoming vehicular emission standards like Bharat Stage 6 (BS-VI), which may realize the low  $NO_x$ , VOC-limited setting without a lockdown, and lead to an inadvertent rise in ozone and LVOOA. The use of double PMF demonstrated in this study has clear implications to improve interpretation of the sources of organic aerosols and black carbon, which can aid future work in this domain.

### CRediT authorship contribution statement

Chirag Manchanda: Methodology, Software, Formal analysis, Writing - original draft, Investigation, Visualization. Mayank Kumar: Conceptualization, Methodology, Writing - review & editing, Supervision, Resources, Project administration, Funding acquisition. Vikram Singh: Methodology, Writing - review & editing, Supervision, Resources, Funding acquisition. Mohd Faisal: Formal analysis, Investigation, Data curation. Naba Hazarika: Data curation, Investigation. Ashutosh Shukla: Validation, Writing - review & editing. Vipul Lalchandani: Validation, Writing - review & editing. Vikas Goel: Investigation, Data curation. Navaneeth Thamban: Validation. Dilip Ganguly: Resources, Data curation. Sachchida Nand Tripathi: Conceptualization, Methodology, Supervision, Resources, Project administration.

# **Declaration of Competing Interest**

The authors declare that they have no known competing financial interests or personal relationships that could have appeared to influence the work reported in this paper.

# Acknowledgments

The authors would like to acknowledge the IRD Grand Challenge Project grant, IIT Delhi (Grant No. IITD/IRD/MI01810G), Ministery of Human Resource Development (MHRD), Government of India and the Central Pollution Control Board (CPCB), Government of India (Grant No. AQM/Source Apportionment EPC project/2017), for the funding support to carry out this project.

#### Appendix A. Supplementary material

Supplementary data to this article can be found online at  $\frac{\text{https:}}{\text{doi.}}$  org/10.1016/j.envint.2021.106541.

#### References

- Aiken, A.C., Salcedo, D., Cubison, M.J., Huffman, J.A., DeCarlo, P.F., Ulbrich, I.M., Docherty, K.S., Sueper, D., Kimmel, J.R., Worsnop, D.R., Trimborn, A., Northway, M., Stone, E.A., Schauer, J.J., Volkamer, R.M., Fortner, E., de Foy, B., Wang, J., Laskin, A., Shutthanandan, V., Zheng, J., Zhang, R., Gaffney, J., Marley, N. A., Paredes-Miranda, G., Arnott, W.P., Molina, L.T., Sosa, G., Jimenez, J.L., 2009. Mexico City aerosol analysis during MILAGRO using high resolution aerosol mass spectrometry at the urban supersite (T0) Part 1: Fine particle composition and organic source apportionment. Atmos. Chem. Phys. 9 (17), 6633–6653. https://doi.org/10.5194/acp-9-6633-200910.5194/acp-9-6633-2009-supplement.
- Almeida, S.M., Pio, C.A., Freitas, M.C., Reis, M.A., Trancoso, M.A., 2006. Source apportionment of atmospheric urban aerosol based on weekdays/weekend variability: evaluation of road re-suspended dust contribution. Atmos. Environ. 40 (11), 2058–2067. https://doi.org/10.1016/j.atmosenv.2005.11.046.
- Bao, R., Zhang, A., 2020. Does lockdown reduce air pollution? Evidence from 44 cities in northern China. Sci. Total Environ. 731, 139052. https://doi.org/10.1016/j. scitoteny.2020.139052
- Brown, S., Lee, T., Roberts, P., Collett, J., 2016. Wintertime Residential Biomass Burning in Las Vegas, Nevada; Marker Components and Apportionment Methods. Atmosphere (Basel). 7, 58. https://doi.org/10.3390/atmos7040058.
- Bullock, P., Gregory, P.J., 1991. In: Soils in the Urban Environment. Blackwell Publishing Ltd., Oxford, UK, pp. 1–4. https://doi.org/10.1002/9781444310603.ch1.
- Burr, M.J., Zhang, Y., 2011. Source apportionment of fine particulate matter over the Eastern U.S. Part I: source sensitivity simulations using CMAQ with the Brute Force method. Atmos. Pollut. Res. 2 (3), 300–317. https://doi.org/10.5094/ APR.2011.036.
- Central Electricity Authority, 2012. Report of The Group for Studying Range of Blending of Imported Coal with Domestic Coal. New Delhi.
- Chakraborty, A., Mandariya, A.K., Chakraborti, R., Gupta, T., Tripathi, S.N., 2018. Realtime chemical characterization of post monsoon organic aerosols in a polluted urban city: Sources, composition, and comparison with other seasons. Environ. Pollut. 232, 310–321. https://doi.org/10.1016/j.envpol.2017.09.079.
- Chandra, A., Chandra, H., 2004. Impact of Indian and imported coal on Indian thermal power plants. J. Sci. Ind. Res. (India) 63, 156–162.
- Csavina, J., Field, J., Félix, O., Corral-Avitia, A.Y., Sáez, A.E., Betterton, E.A., 2014. Effect of wind speed and relative humidity on atmospheric dust concentrations in semi-arid climates. Sci. Total Environ. 487, 82–90. https://doi.org/10.1016/j. scitotenv.2014.03.138.
- DeCarlo, P.F., Ulbrich, I.M., Crounse, J., de Foy, B., Dunlea, E.J., Aiken, A.C., Knapp, D., Weinheimer, A.J., Campos, T., Wennberg, P.O., Jimenez, J.L., 2010. Investigation of the sources and processing of organic aerosol over the Central Mexican Plateau from aircraft measurements during MILAGRO. Atmos. Chem. Phys. 10 (12), 5257–5280. https://doi.org/10.5194/acp-10-5257-201010.5194/acp-10-5257-2010-supplement.
- DeWitt, H.L., Hellebust, S., Temime-Roussel, B., Ravier, S., Polo, L., Jacob, V., Buisson, C., Charron, A., André, M., Pasquier, A., Besombes, J.L., Jaffrezo, J.L., Wortham, H., Marchand, N., 2015. Near-highway aerosol and gas-phase measurements in a high-diesel environment. Atmos. Chem. Phys. 15 (8), 4373–4387. https://doi.org/10.5194/acp-15-4373-201510.5194/acp-15-4373-2015
- Dhaka, S.K., Chetna, Kumar, V., Panwar, V., Dimri, A.P., Singh, N., Patra, P.K., Matsumi, Y., Takigawa, M., Nakayama, T., Yamaji, K., Kajino, M., Misra, P., Hayashida, S., 2020. PM2.5 diminution and haze events over Delhi during the COVID-19 lockdown period: an interplay between the baseline pollution and meteorology. Sci. Rep. 10 (1) https://doi.org/10.1038/s41598-020-70179-8.
- Duan, J., Tan, J., 2013. Atmospheric heavy metals and Arsenic in China: Situation, sources and control policies. Atmos. Environ. 74, 93–101. https://doi.org/10.1016/ j.atmosenv.2013.03.031.
- Dyke, P.H., Sutton, M., Wood, D., Marshall, J., 2007. Investigations on the effect of chlorine in lubricating oil and the presence of a diesel oxidation catalyst on PCDD/F releases from an internal combustion engine. Chemosphere 67 (7), 1275–1286. https://doi.org/10.1016/j.chemosphere.2006.12.010.
- Dzepina, K., Volkamer, R.M., Madronich, S., Tulet, P., Ulbrich, I.M., Zhang, Q., Cappa, C. D., Ziemann, P.J., Jimenez, J.L., 2009. Evaluation of recently-proposed secondary organic aerosol models for a case study in Mexico City. Atmos. Chem. Phys. 9 (15), 5681–5709. https://doi.org/10.5194/acp-9-5681-200910.5194/acp-9-5681-2009-cupalement.
- Fehsenfeld, F., 2004. Chapter 5, in: Howard McMurry, P., F. Shepherd, M., S. Vickery, J. (Eds.), Particulate Matter Science for Policy Makers: A NARSTO Assessment. Cambridge University Press.
- Finlayson-Pitts, B.J., Pitts, J.N., 1993. Atmospheric Chemistry of Tropospheric Ozone Formation: Scientific and Regulatory Implications. Air Waste 43 (8), 1091–1100. https://doi.org/10.1080/1073161X.1993.10467187.
- Fitch, J., 2019. Copper and Your Diesel Engine Oils [WWW Document]. Mach. Lubr.
  Noria Corp. URL www.machinerylubrication.com/Read/646/copper-diesel-engine
- Gani, S., Bhandari, S., Seraj, S., Wang, D.S., Patel, K., Soni, P., Arub, Z., Habib, G., Hildebrandt Ruiz, L., Apte, J.S., 2019. Submicron aerosol composition in the world's

- most polluted megacity: the Delhi Aerosol Supersite study. Atmos. Chem. Phys. 19 (10), 6843-6859. https://doi.org/10.5194/acp-19-6843-201910.5194/acp-19-
- Gerlofs-Nijland, M.E., Bokkers, B.G.H., Sachse, H., Reijnders, J.J.E., Gustafsson, M. Boere, A.J.F., Fokkens, P.F.H., Leseman, D.L.A.C., Augsburg, K., Cassee, F.R., 2019. Inhalation toxicity profiles of particulate matter: a comparison between brake wear with other sources of emission. Inhal. Toxicol. 31 (3), 89–98. https://doi.org 10.1080/08958378.2019.1606365
- Gianini, M.F.D., Gehrig, R., Fischer, A., Ulrich, A., Wichser, A., Hueglin, C., 2012. Chemical composition of PM10 in Switzerland: An analysis for 2008/2009 and changes since 1998/1999. Atmos. Environ. 54, 97-106. https://doi.org/10.1016/j.
- Goel, V., Hazarika, N., Kumar, M., Singh, V., Thamban, N.M., Tripathi, S.N., 2021. Variations in Black Carbon concentration and sources during COVID-19 lockdown in Delhi. Chemosphere 270, 129435. https://doi.org/10.1016/j
- Goldstein, I.S., 2018. Organic Chemicals from Biomass. CRC Press.
- Google LLC, 2020. Google COVID-19 Community Mobility Reports.
- Grigoratos, T., Martini, G., 2015. Brake wear particle emissions: a review. Environ. Sci. Pollut. Res. 22 (4), 2491-2504. https://doi.org/10.1007/s11356-014-3696-8.
- Gupta, A.K., Karar, K., Srivastava, A., 2007. Chemical mass balance source apportionment of PM10 and TSP in residential and industrial sites of an urban region of Kolkata, India. J. Hazard. Mater. 142 (1-2), 279-287. https://doi.org/10.1016/j.
- Gupta, I., Salunkhe, A., Kumar, R., 2012. Source apportionment of PM10 by positive matrix factorization in urban area of Mumbai, India. Sci. World J. 2012 https://doi. org/10.1100/2012/585791.
- Hao, L.Q., Kortelainen, A., Romakkaniemi, S., Portin, H., Jaatinen, A., Leskinen, A., Komppula, M., Miettinen, P., Sueper, D., Pajunoja, A., Smith, J.N., Lehtinen, K.E.J., Worsnop, D.R., Laaksonen, A., Virtanen, A., 2014. Atmospheric submicron aerosol composition and particulate organic nitrate formation in a boreal forestland-urban mixed region. Atmos. Chem. Phys. 14 (24), 13483-13495. https://doi.org/10.5194/ acp-14-13483-201410.5194/acp-14-13483-2014-supplement
- Hien, P.D., Binh, N.T., Truong, Y., Ngo, N.T., Sieu, L.N., 2001. Comparative receptor modelling study of TSP, PM2 and PM2-10 in Ho Chi Minh City. Atmos. Environ. 35 (15), 2669-2678. https://doi.org/10.1016/S1352-2310(00)0057
- Huang, R.-J., Zhang, Y., Bozzetti, C., Ho, K.-F., Cao, J.-J., Han, Y., Daellenbach, K.R., Slowik, J.G., Platt, S.M., Canonaco, F., Zotter, P., Wolf, R., Pieber, S.M., Bruns, E.A., Crippa, M., Ciarelli, G., Piazzalunga, A., Schwikowski, M., Abbaszade, G., Schnelle-Kreis, J., Zimmermann, R., An, Z., Szidat, S., Baltensperger, U., Haddad, I.E., Prévôt, A.S.H., 2014. High secondary aerosol contribution to particulate pollution during haze events in China. Nature 514 (7521), 218-222. https://doi.org/10.1038/
- Jaiprakash, Singhai, A., Habib, G., Raman, R.S., Gupta, T., 2017. Chemical characterization of PM1.0 aerosol in Delhi and source apportionment using positive matrix factorization. Environ. Sci. Pollut. Res. 24 (1), 445–462. https://doi.org/ s11356-016-7708-8.
- Jayamurugan, R., Kumaravel, B., Palanivelraja, S., Chockalingam, M.P., 2013. Influence of Temperature, Relative Humidity and Seasonal Variability on Ambient Air Quality in a Coastal Urban Area, Int. J. Atmos. Sci. 2013, 1–7, https://doi.org/10.1155/
- Jethva, H., Torres, O., Field, R.D., Lyapustin, A., Gautam, R., Kayetha, V., 2019. Connecting Crop Productivity, Residue Fires, and Air Quality over Northern India. Sci. Rep. 9 (1) https://doi.org/10.1038/s41598-019-52799-2
- Jimenez, J.L., Canagaratna, M.R., Donahue, N.M., Prevot, A.S.H., Zhang, Q., Kroll, J.H., DeCarlo, P.F., Allan, J.D., Coe, H., Ng, N.L., Aiken, A.C., Docherty, K.S., Ulbrich, I. M., Grieshop, A.P., Robinson, A.L., Duplissy, J., Smith, J.D., Wilson, K.R., Lanz, V.A., Hueglin, C., Sun, Y.L., Tian, J., Laaksonen, A., Raatikainen, T., Rautiainen, J., Vaattovaara, P., Ehn, M., Kulmala, M., Tomlinson, J.M., Collins, D.R., Cubison, M.J., Dunlea, J., Huffman, J.A., Onasch, T.B., Alfarra, M.R., Williams, P.I., Bower, K., Kondo, Y., Schneider, J., Drewnick, F., Borrmann, S., Weimer, S., Demerjian, K., Salcedo, D., Cottrell, L., Griffin, R., Takami, A., Miyoshi, T., Hatakeyama, S., Shimono, A., Sun, J.Y., Zhang, Y.M., Dzepina, K., Kimmel, J.R., Sueper, D., Jayne, J. T., Herndon, S.C., Trimborn, A.M., Williams, L.R., Wood, E.C., Middlebrook, A.M., Kolb, C.E., Baltensperger, U., Worsnop, D.R., 2009. Evolution of Organic Aerosols in the Atmosphere. Science (80-) 326 (5959), 1525-1529. https://doi.org/10.1126/
- Julander, A., Lundgren, L., Skare, L., Grandér, M., Palm, B., Vahter, M., Lidén, C., 2014. Formal recycling of e-waste leads to increased exposure to toxic metals: An occupational exposure study from Sweden. Environ. Int. 73, 243-251. https://doi. 10.1016/j.envint.2014.07.006
- Khare, P., Baruah, B.P., 2010. Elemental characterization and source identification of PM2.5 using multivariate analysis at the suburban site of North-East India. Atmos. Res. 98 (1), 148-162. https://doi.org/10.1016/j.atmosres.2010.07.001
- Kothai, P., Saradhi, I.V., Pandit, G.G., Markwitz, A., Puranik, V.D., 2011. Chemical Characterization and Source Identification of Particulate Matter at an Urban Site of Navi Mumbai, India. Aerosol Air Qual. Res. 11 (5), 560-569. https://doi.org/
- Kumar, P., Hama, S., Omidvarborna, H., Sharma, A., Sahani, J., Abhijith, K.V., Debele, S. E., Zavala-Reyes, J.C., Barwise, Y., Tiwari, A., 2020. Temporary reduction in fine particulate matter due to 'anthropogenic emissions switch-off' during COVID-19 lockdown in Indian cities. Sustain. Cities Soc. 62, 102382. https://doi.org/10.1016/
- Kumari, P., Toshniwal, D., 2020. Impact of lockdown measures during COVID-19 on air quality- A case study of India. Int. J. Environ. Health Res. 00, 1-8. https://doi.org/ 10.1080/09603123.2020.1778646.

- LANCE FIRMS, 2020. MODIS Collection 6 [WWW Document]. NASA's Earth Sci. Data Inf. Syst. https://doi.org/10.5067/firms/modis/mcd14dl.nrt.006.
- Lee, S., Liu, W., Wang, Y., Russell, A.G., Edgerton, E.S., 2008. Source apportionment of PM2.5: Comparing PMF and CMB results for four ambient monitoring sites in the southeastern United States. Atmos. Environ. 42 (18), 4126-4137. https://doi.org/ 10.1016/j.atmosenv.2008.01.025.
- Lee, T., Sullivan, A.P., Mack, L., Jimenez, J.L., Kreidenweis, S.M., Onasch, T.B., Worsnop, D.R., Malm, W., Wold, C.E., Hao, W.M., Collett, J.L., 2010. Chemical Smoke Marker Emissions During Flaming and Smoldering Phases of Laboratory Open Burning of Wildland Fuels. Aerosol Sci. Technol. 44 (9), i-v. https://doi.org/
- Li, J., Liu, Q., Li, Y., Liu, T., Huang, D., Zheng, J., Zhu, W., Hu, M., Wu, Y., Lou, S., Hallquist, Å.M., Hallquist, M., Chan, C.K., Canonaco, F., Prévôt, A.S.H., Fung, J.C.H., Lau, A.K.H., Yu, J.Z., 2019. Characterization of Aerosol Aging Potentials at Suburban Sites in Northern and Southern China Utilizing a Potential Aerosol Mass (Go:PAM) Reactor and an Aerosol Mass Spectrometer. J. Geophys. Res. Atmos. 124 (10), 5629-5649. https://doi.org/10.1029/2018JD029904
- Li, J., Pósfai, M., Hobbs, P.V., Buseck, P.R., 2003. Individual aerosol particles from biomass burning in southern Africa: 2, Compositions and aging of inorganic particles. J. Geophys. Res. Atmos. 108 (D13), n/a-n/a. https://doi.org/10.1029/
- Li, L., Li, Q., Huang, L., Wang, Q., Zhu, A., Xu, J., Liu, Ziyi, Li, H., Shi, L., Li, R., Azari, M., Wang, Y., Zhang, X., Liu, Zhiqiang, Zhu, Y., Zhang, K., Xue, S., Ooi, M.C.G., Zhang, D., Chan, A., 2020. Air quality changes during the COVID-19 lockdown over the Yangtze River Delta Region: An insight into the impact of human activity pattern changes on air pollution variation. Sci. Total Environ. 732, 139282. https://doi.org/ 10.1016/i.scitotenv.2020.139282.
- Liggio, J., Li, S.M., 2013. A new source of oxygenated organic aerosol and oligomers.
- Atmos. Chem. Phys. 13, 2989–3002. https://doi.org/10.5194/acp-13-2989-2013. Lin, C., Ceburnis, D., Hellebust, S., Buckley, P., Wenger, J., Canonaco, F., Prévôt, A.S.H., Huang, R.-J., O'Dowd, C., Ovadnevaite, J., 2017. Characterization of Primary Organic Aerosol from Domestic Wood, Peat, and Coal Burning in Ireland. Environ. Sci. Technol. 51 (18), 10624-10632. https://doi.org/10.1021/acs. est.7b0192610.1021/acs.est.7b01926.s001.
- Lv, Z., Wang, X., Deng, F., Ying, Q., Archibald, A.T., Jones, R.L., Ding, Y., Cheng, Y., Fu, M., Liu, Y., Man, H., Xue, Z., He, K., Hao, J., Liu, H., 2020. Significant reduced traffic in Beijing failed to relieve haze pollution during the COVID-19 lockdown: implications for haze mitigation.
- Lyyränen, J., Jokiniemi, J., Kauppinen, E.I., Joutsensaari, J., 1999. Aerosol characterisation in medium-speed diesel engines operating with heavy fuel oils. J. Aerosol Sci. 30 (6), 771–784. https://doi.org/10.1016/S0021-8502(98)00763-0.
- Mahato, S., Pal, S., Ghosh, K.G., 2020. Effect of lockdown amid COVID-19 pandemic on air quality of the megacity Delhi, India. Sci. Total Environ. 730, 139086. https://doi. org/10.1016/i.scitotenv.2020.139086
- Mohr, C., Huffman, J.A., Cubison, M.J., Aiken, A.C., Docherty, K.S., Kimmel, J.R., Ulbrich, I.M., Hannigan, M., Jimenez, J.L., 2009. Characterization of Primary Organic Aerosol Emissions from Meat Cooking, Trash Burning, and Motor Vehicles with High-Resolution Aerosol Mass Spectrometry and Comparison with Ambient and Chamber Observations. Environ. Sci. Technol. 43 (7), 2443-2449. https://doi.org/ 10 1021/es8011518
- Monks, P.S., Archibald, A.T., Colette, A., Cooper, O., Coyle, M., Derwent, R., Fowler, D., Granier, C., Law, K.S., Mills, G.E., Stevenson, D.S., Tarasova, O., Thouret, V., von Schneidemesser, E., Sommariva, R., Wild, O., Williams, M.L., 2015. Tropospheric ozone and its precursors from the urban to the global scale from air quality to shortlived climate forcer. Atmos. Chem. Phys. 15, 8889–8973. https://doi.org/10.5194/ n-15-8889-2015
- Negi, B.S., Sadasivan, S., Mishra, U.C., 1967. Aerosol composition and sources in Urban areas in India. Atmos. Environ. 21 (6), 1259-1266. https://doi.org/10.1016/0004 6981(67)90072-8.
- Ng, N.L., Canagaratna, M.R., Jimenez, J.L., Chhabra, P.S., Seinfeld, J.H., Worsnop, D.R., 2011. Changes in organic aerosol composition with aging inferred from aerosol mass spectra. Atmos. Chem. Phys. 11 (13), 6465-6474. https://doi.org/10.5194/acp-11-6465-201110.5194/acp-11-6465-2011-supplement.
- Obernberger, I., Brunner, T., Barnthaler, G., 2006. Chemical properties of solid biofuelssignificance and impact. Biomass Bioenergy 30 (11), 973-982. https://doi.org/ 10.1016/j.biombioe.2006.06.011
- Ohta, S., Okita, T., 1990. A chemical characterization of atmospheric aerosol in Sapporo. Atmos. Environ. Part A. Gen. Top. 24 (4), 815-822. https://doi.org/10.1016/
- Oxford COVID-19 Government Response Tracker, 2020. Oxford COVID-19 Government Response Tracker (OxCGRT) [WWW Document]. URL https://www.bsg.ox.ac.uk earch/research-projects/coronavirus-government-response-tracker (accessed 5.31.20)
- Paatero, P., 1999. The Multilinear Engine—A Table-Driven, Least Squares Program for Solving Multilinear Problems, Including the n -Way Parallel Factor Analysis Model. J. Comput. Graph. Stat. 8 (4), 854-888. https://doi.org/10.1080 10618600.1999.10474853
- Paatero, P., 1997. Least squares formulation of robust non-negative factor analysis. Chemom. Intell. Lab. Syst. 37 (1), 23-35. https://doi.org/10.1016/S0169-7439(96)
- Paatero, P., Tapper, U., 1994. Positive matrix factorization: A non-negative factor model with optimal utilization of error estimates of data values. Environmetrics 5 (2), 111-126. https://doi.org/10.1002/(ISSN)1099-095X10.1002/env.v5:210.1002/ env.3170050203.

- Pant, P., Harrison, R.M., 2012. Critical review of receptor modelling for particulate matter: A case study of India. Atmos. Environ. 49, 1–12. https://doi.org/10.1016/j. atmosenv.2011.11.060.
- Parekh, P.P., Ghauri, B., Siddiqi, Z.R., Husain, L., 1967. The use of chemical and statistical methods to identify sources of selected elements in ambient air aerosols in Karachi, Pakistan. Atmos. Environ. 21 (6), 1267–1274. https://doi.org/10.1016/ 0004\_608167900073 X
- Petit, J.-E., Favez, O., Sciare, J., Canonaco, F., Croteau, P., Močnik, G., Jayne, J., Worsnop, D., Leoz-Garziandia, E., 2014. Submicron aerosol source apportionment of wintertime pollution in Paris, France by double positive matrix factorization (PMF<sup>2</sup>) using an aerosol chemical speciation monitor (ACSM) and a multi-wavelength Aethalometer. Atmos. Chem. Phys. 14 (24), 13773–13787. https://doi.org/10.5194/acp-14-13773-201410.5194/acp-14-13773-2014-supplement
- POSOCO, 2020. All-India Maximum Demand and Energy Met during Management of COVID -19 in comparison to 2019.
- Rai, P., Furger, M., El Haddad, I., Kumar, V., Wang, L., Singh, A., Dixit, K., Bhattu, D., Petit, J.-E., Ganguly, D., Rastogi, N., Baltensperger, U., Tripathi, S.N., Slowik, J.G., Prévôt, A.S.H., 2020a. Real-time measurement and source apportionment of elements in Delhi's atmosphere. Sci. Total Environ. 742, 140332. https://doi.org/10.1016/j.scitotenv.2020.140332.
- Rai, P., Furger, M., Slowik, J.G., Canonaco, F., Fröhlich, R., Hüglin, C., Minguillón, M.C., Petterson, K., Baltensperger, U., Prévôt, A.S.H., 2020b. Source apportionment of highly time-resolved elements during a firework episode from a rural freeway site in Switzerland. Atmos. Chem. Phys. 20 (3), 1657–1674. https://doi.org/10.5194/acp-20-1657-202010.5194/acp-20-1657-2020-supplement.
- Reche, C., Viana, M., Amato, F., Alastuey, A., Moreno, T., Hillamo, R., Teinilä, K., Saarnio, K., Seco, R., Peñuelas, J., Mohr, C., Prévôt, A.S.H., Querol, X., 2012. Biomass burning contributions to urban aerosols in a coastal Mediterranean City. Sci. Total Environ. 427–428, 175–190. https://doi.org/10.1016/j.scitotenv.2012.04.012
- Reddy, M.S., Basha, S., Joshi, H.V., Jha, B., 2005. Evaluation of the emission characteristics of trace metals from coal and fuel oil fired power plants and their fate during combustion. J. Hazard. Mater. 123 (1-3), 242–249. https://doi.org/10.1016/ j.jhazmat.2005.04.008.
- Roy, R., Agarwal, V., 2020. Millions of Indians Are Fleeing Cities, Raising Fears of a Coronavirus 'Land Mine' in Villages. Wall Str. J.
- Rudnick, L.R., 2017. Lubricant Additives: Chemistry and Applications. CRC Press, Taylor & Francis Group.
- Sandradewi, J., Prévôt, A.S.H., Szidat, S., Perron, N., Alfarra, M.R., Lanz, V.A., Weingartner, E., Baltensperger, U., 2008. Using Aerosol Light Absorption Measurements for the Quantitative Determination of Wood Burning and Traffic Emission Contributions to Particulate Matter. Environ. Sci. Technol. 42 (9), 3316–3323. https://doi.org/10.1021/es702253m.
- Sarkar, S., 2009. Fuels and Combustion, CRC Press.
- Seinfeld, J.H., Pandis, S.N., 2006. Atmospheric Chemistry and Physics: From Air Pollution to Climate Change, 2nd ed. John Wiley & Sons, New York.
- Seinfeld, J.H., 2004. Air pollution: A half century of progress. AIChE J. 50 (6), 1096–1108. https://doi.org/10.1002/(ISSN)1547-590510.1002/aic.v50:610.1002/aic.10102.
- Selvam, S., Muthukumar, P., Venkatramanan, S., Roy, P.D., Manikanda Bharath, K., Jesuraja, K., 2020. SARS-CoV-2 pandemic lockdown: Effects on air quality in the industrialized Gujarat state of India. Sci. Total Environ. 737, 140391. https://doi. org/10.1016/j.scitotenv.2020.140391.
- Sharma, H., Jain, V.K., Khan, Z.H., 2007. Characterization and source identification of polycyclic aromatic hydrocarbons (PAHs) in the urban environment of Delhi. Chemosphere 200 (2), 302–310. https://doi.org/10.1016/j. chemosphere.2006.05.003.
- Sharma, N., Prakash, R., Srivastava, A., Sadana, U.S., Acharya, R., Prakash, N.T., Reddy, A.V.R., 2009. Profile of selenium in soil and crops in seleniferous area of Punjab, India by neutron activation analysis. J. Radioanal. Nucl. Chem. 281 (1), 59–62. https://doi.org/10.1007/s10967-009-0082-y.
- Sharma, S.K., Mandal, T.K., Jain, S., Saraswati, Sharma, A., Saxena, M., 2016. Source Apportionment of PM2.5 in Delhi, India Using PMF Model. Bull. Environ. Contam. Toxicol. 97 (2). 286–293. https://doi.org/10.1007/s00128-016-1836-1
- Toxicol. 97 (2), 286–293. https://doi.org/10.1007/s00128-016-1836-1. Shridhar, V., Khillare, P.S., Agarwal, T., Ray, S., 2010. Metallic species in ambient particulate matter at rural and urban location of Delhi. J. Hazard. Mater. 175 (1-3), 600–607. https://doi.org/10.1016/j.jhazmat.2009.10.047.
- Sicard, P., De Marco, A., Agathokleous, E., Feng, Z., Xu, X., Paoletti, E., Rodriguez, J.J.D., Calatayud, V., 2020. Amplified ozone pollution in cities during the COVID-19 lockdown. Sci. Total Environ. 735, 139542. https://doi.org/10.1016/j. scitotenv.2020.139542.
- Sohrabi, C., Alsafi, Z., O'Neill, N., Khan, M., Kerwan, A., Al-Jabir, A., Iosifidis, C., Agha, R., 2020. World Health Organization declares global emergency: A review of the 2019 novel coronavirus (COVID-19). Int. J. Surg. 76, 71–76. https://doi.org/ 10.1016/j.ijsu.2020.02.034
- Spencer, M.T., Shields, L.G., Sodeman, D.A., Toner, S.M., Prather, K.A., 2006. Comparison of oil and fuel particle chemical signatures with particle emissions from heavy and light duty vehicles. Atmos. Environ. 40 (27), 5224–5235. https://doi.org/ 10.1016/j.atmosenv.2006.04.011.
- Srivastava, S., Kumar, A., Bauddh, K., Gautam, A.S., Kumar, S., 2020. 21-Day Lockdown in India Dramatically Reduced Air Pollution Indices in Lucknow and New Delhi,

- India. Bull. Environ. Contam. Toxicol. 105 (1), 9–17. https://doi.org/10.1007/s00128-020-02895-w.
- Sun, J., Shen, Z., Zhang, L., Lei, Y., Gong, X., Zhang, Q., Zhang, T., Xu, H., Cui, S., Wang, Q., Cao, J., Tao, J., Zhang, N., Zhang, R., 2019. Chemical source profiles of urban fugitive dust PM2.5 samples from 21 cities across China. Sci. Total Environ. 649, 1045–1053. https://doi.org/10.1016/j.scitotenv.2018.08.374.
- Sun, Y., Du, W., Fu, P., Wang, Q., Li, J., Ge, X., Zhang, Q., Zhu, C., Ren, L., Xu, W., Zhao, J., Han, T., Worsnop, D.R., Wang, Z., 2016. Primary and secondary aerosols in Beijing in winter: sources, variations and processes. Atmos. Chem. Phys. 16 (13), 8309–8329. https://doi.org/10.5194/acp-16-8309-201610.5194/acp-16-8309-2016-supplement.
- Sweet, C.W., Vermette, S.J., Landsberger, S., 1993. Sources of toxic trace elements in urban air in Illinois. Environ. Sci. Technol. 27 (12), 2502–2510. https://doi.org/ 10.1021/es00048a030.
- Thorpe, A., Harrison, R.M., 2008. Sources and properties of non-exhaust particulate matter from road traffic: A review. Sci. Total Environ. 400 (1-3), 270–282. https://doi.org/10.1016/j.scitotenv.2008.06.007.
- Tobías, A., Carnerero, C., Reche, C., Massagué, J., Via, M., Minguillón, M.C., Alastuey, A., Querol, X., 2020. Changes in air quality during the lockdown in Barcelona (Spain) one month into the SARS-CoV-2 epidemic. Sci. Total Environ. 726, 138540. https://doi.org/10.1016/j.scitotenv.2020.138540.
- Ulbrich, I.M., Canagaratna, M.R., Zhang, Q., Worsnop, D.R., Jimenez, J.L., 2009. Interpretation of organic components from Positive Matrix Factorization of aerosol mass spectrometric data. Atmos. Chem. Phys. 9 (9), 2891–2918. https://doi.org/10.5194/acp-9-2891-200910.5194/acp-9-2891-2009-supplement.
- Vehlow, J., Bergfeldt, B., Hunsinger, H., Scifert, H., Mark, F.E., 2003. Bromine in waste incineration partitioning and influence on metal volatilisation. Environ. Sci. Pollut. Res. 10 (5), 329–334. https://doi.org/10.1065/espr2003.02.147.
- Volkamer, R., Jimenez, J.L., San Martini, F., Dzepina, K., Zhang, Q., Salcedo, D., Molina, L.T., Worsnop, D.R., Molina, M.J., 2006. Secondary organic aerosol formation from anthropogenic air pollution: Rapid and higher than expected. Geophys. Res. Lett. 33, L17811. https://doi.org/10.1029/2006GL026899.
- Vossler, Teri, Černikovský, Libor, Novák, Jiří, Williams, Ronald, 2016. Source apportionment with uncertainty estimates of fine particulate matter in Ostrava, Czech Republic using Positive Matrix Factorization. Atmos. Pollut. Res. 7 (3), 503–512. https://doi.org/10.1016/j.apr.2015.12.004.
- Warner, J.X., Dickerson, R.R., Wei, Z., Strow, L.L., Wang, Y., Liang, Q., 2017. Increased atmospheric ammonia over the world's major agricultural areas detected from space. Geophys. Res. Lett. 44 (6), 2875–2884. https://doi.org/10.1002/2016GL072305.
- Watson, John G., Chow, Judith C., 2015. In: Introduction to Environmental Forensics. Elsevier, pp. 677–706. https://doi.org/10.1016/B978-0-12-404696-2.00020-5.
- Wilson, Wm. E., Levy, Arthur, Wimmer, D.B., 1972. A Study of Sulfur Dioxide in Photochemical Smog. J. Air Pollut. Control Assoc. 22 (1), 27–32. https://doi.org/ 10.1080/00022470.1972.10469605.
- Wu, Gamber, Sun, 2020. Does Wuhan Need to be in Lockdown during the Chinese Lunar New Year? Int. J. Environ. Res. Public Health 17, 1002. https://doi.org/10.3390/ ijerph17031002.
- Yadav, Ravi, Korhale, N., Anand, V., Rathod, A., Bano, S., Shinde, R., Latha, R., Sahu, S. K., Murthy, B.S., Beig, Gufran, 2020. COVID-19 lockdown and air quality of SAFAR-India metro cities. Urban Clim. 34, 100729. https://doi.org/10.1016/j.uclim.2020.100729.
- Zhang, Q., Rami Alfarra, M., Worsnop, D.R., Allan, J.D., Coe, H., Canagaratna, M.R., Jimenez, J.L., 2005a. Deconvolution and quantification of hydrocarbon-like and oxygenated organic aerosols based on aerosol mass spectrometry. Environ. Sci. Technol. 39 (13), 4938–4952. https://doi.org/10.1021/es048568l10.1021/es048568l.s001.
- Zhang, Q., Worsnop, D.R., Canagaratna, M.R., Jimenez, J.L., 2005b. Hydrocarbon-like and oxygenated organic aerosols in Pittsburgh: insights into sources and processes of organic aerosols. Atmos. Chem. Phys. 5, 3289–3311. https://doi.org/10.5194/acp-5-3289-2005.
- Zhang, T., Cao, J.J., Tie, X.X., Shen, Z.X., Liu, S.X., Ding, H., Han, Y.M., Wang, G.H., Ho, K.F., Qiang, J., Li, W.T., 2011. Water-soluble ions in atmospheric aerosols measured in Xi'an, China: Seasonal variations and sources. Atmos. Res. 102 (1-2), 110–119. https://doi.org/10.1016/j.atmosres.2011.06.014.
- Zhao, S., Duan, Y., Chen, L., Li, Y., Yao, T., Liu, S., Liu, M., Lu, J., 2017. Study on emission of hazardous trace elements in a 350 MW coal-fired power plant. Part 2. arsenic, chromium, barium, manganese, lead. Environ. Pollut. 226, 404–411. https://doi.org/10.1016/j.envpol.2017.04.009.
- Zheng, H., Kong, S., Chen, N., Yan, Y., Liu, D., Zhu, B., Xu, K., Cao, W., Ding, Q., Lan, B., Zhang, Z., Zheng, M., Fan, Z., Cheng, Y., Zheng, S., Yao, L., Bai, Y., Zhao, T., Qi, S., 2020. Significant changes in the chemical compositions and sources of PM2.5 in Wuhan since the city lockdown as COVID-19. Sci. Total Environ. 739, 140000. https://doi.org/10.1016/j.scitotenv.2020.140000.
- Zhu, Q., Huang, X.-F., Cao, L.-M., Wei, L.-T., Zhang, B., He, L.-Y., Elser, M., Canonaco, F., Slowik, J.G., Bozzetti, C., El-Haddad, I., Prévôt, A.S.H., 2018. Improved source apportionment of organic aerosols in complex urban air pollution using the multilinear engine (ME-2). Atmos. Meas. Tech. 11 (2), 1049–1060. https://doi.org/10.5194/amt-11-1049-2018-supplement.
- Zoller, W.H., Gladney, E.S., Gordon, G.E., Bors, J.J., 1974. Emissions of trace elements from coal fired power plants. Trace Subst. Environ. Heal. 8.